NASA/TM—2008-215157 AIAA–2008–50

Spectral Separation of the Turbofan Engine Coherent Combustion Noise Component

Jeffrey Hilton Miles
Glenn Research Center, Cleveland, Ohio

May 2008

NASA STI Program . . . in Profile

Since its founding, NASA has been dedicated to the advancement of aeronautics and space science. The NASA Scientific and Technical Information (STI) program plays a key part in helping NASA maintain this important role.

The NASA STI Program operates under the auspices of the Agency Chief Information Officer. It collects, organizes, provides for archiving, and disseminates NASA's STI. The NASA STI program provides access to the NASA Aeronautics and Space Database and its public interface, the NASA Technical Reports Server, thus providing one of the largest collections of aeronautical and space science STI in the world. Results are published in both non-NASA channels and by NASA in the NASA STI Report Series, which includes the following report types:

- TECHNICAL PUBLICATION. Reports of completed research or a major significant phase of research that present the results of NASA programs and include extensive data or theoretical analysis. Includes compilations of significant scientific and technical data and information deemed to be of continuing reference value. NASA counterpart of peer-reviewed formal professional papers but has less stringent limitations on manuscript length and extent of graphic presentations.

- TECHNICAL MEMORANDUM. Scientific and technical findings that are preliminary or of specialized interest, e.g., quick release reports, working papers, and bibliographies that contain minimal annotation. Does not contain extensive analysis.

- CONTRACTOR REPORT. Scientific and technical findings by NASA-sponsored contractors and grantees.

- CONFERENCE PUBLICATION. Collected papers from scientific and technical conferences, symposia, seminars, or other meetings sponsored or cosponsored by NASA.

- SPECIAL PUBLICATION. Scientific, technical, or historical information from NASA programs, projects, and missions, often concerned with subjects having substantial public interest.

- TECHNICAL TRANSLATION. English-language translations of foreign scientific and technical material pertinent to NASA's mission.

Specialized services also include creating custom thesauri, building customized databases, organizing and publishing research results.

For more information about the NASA STI program, see the following:

- Access the NASA STI program home page at *http://www.sti.nasa.gov*

- E-mail your question via the Internet to *help@sti.nasa.gov*

- Fax your question to the NASA STI Help Desk at 301–621–0134

- Telephone the NASA STI Help Desk at 301–621–0390

- Write to:
  NASA Center for AeroSpace Information (CASI)
  7115 Standard Drive
  Hanover, MD 21076–1320

NASA/TM—2008-215157 AIAA–2008–50

Spectral Separation of the Turbofan Engine Coherent Combustion Noise Component

Jeffrey Hilton Miles
Glenn Research Center, Cleveland, Ohio

Prepared for the
46th AIAA Aerospace Sciences Meeting and Exhibit
sponsored by the American Institute of Aeronautics and Astronautics
Reno, Nevada, January 7–10, 2008

National Aeronautics and
Space Administration

Glenn Research Center
Cleveland, Ohio 44135

May 2008

Acknowledgments

The acoustic time histories analyzed herein were made available by Honeywell Aerospace as part of the NASA/Honeywell Engine Validation of Noise and Emissions Reduction Technology (EVNERT) program under provisions of NASA Contract NASA33–01136 from tests conducted by Honeywell Aerospace at the San Tan test site located southeast of Phoenix, Arizona. Special thanks go to Jeff Mendoza and Don Weir for helpful discussions, comments, site figures, and engine installation photos of the test site.

This work was sponsored by the Fundamental Aeronautics Program at the NASA Glenn Research Center.

Level of Review: This material has been technically reviewed by technical management.

Available from

NASA Center for Aerospace Information
7115 Standard Drive
Hanover, MD 21076–1320

National Technical Information Service
5285 Port Royal Road
Springfield, VA 22161

Available electronically at http://gltrs.grc.nasa.gov

Spectral Separation of the Turbofan Engine Coherent Combustion Noise Component

Jeffrey Hilton Miles
National Aeronautics and Space Administration
Cleveland, Ohio 44135

The study of combustion noise from turbofan engines has become more important as other noise sources like the airframe, the fan and the jet are reduced. However, modern engines are based on new materials and a longer history of experience in turbofan engine manufacturing, design, analysis, and optimization, which has led to engines with reduced coherent combustor noise. In addition, the jet mixing noise from near the end of the potential core masks the low-frequency core noise. This makes it necessary to update the coherent output power spectrum method so that the coherent combustion noise spectrum can be determined in spite of its low level. The core noise components of a dual spool turbofan engine (Honeywell TECH977) for engine power settings of 48, 54, and 60 percent were separated by the use of a coherence function. A method has been developed to help identify combustion noise coherence using an aligned and unaligned coherence technique, which enables the validation of low levels of coherence as being due to core noise by identifying the coherence noise floor. A statistical procedure is also used to establish this threshold level. The use of both methods provides a high confidence level for the coherence function values calculated. A source location technique based on adjusting the time delay between the combustor pressure sensor signal and the far-field microphone signal to maximize the coherence and remove as much variation of the phase angle with frequency as possible was used. These techniques make it possible to quantify the weak coherent core noise in the aft quadrant instead of dismissing it as negligible.

While adjusting the time delay to maximize the coherence and minimize the cross-spectrum phase angle variation with frequency, the discovery was made that for the 130^o microphone a 90.027 ms time shift worked best for the frequency band from 0 to 200 Hz while a 86.975 ms time shift worked best for the frequency band from 200 to 400 Hz. Since the 0 to 200 Hz band signal took more time to travel the same distance, it is slower than the 200 to 400 Hz band signal. This suggests the 0 to 200 Hz coherent cross-spectral density band signal is partly due to "indirect" combustion noise attributed to "hot spots" interacting with the turbine. The net travel time of the indirect combustion noise signal from the combustor to the far field is increased since the travel velocity of the hot spots to the turbine and in the turbine is the flow velocity, which is some small fraction of the speed of sound. The indirect combustion noise signal does not travel with the speed of an acoustic wave until it interacts with the turbine. The signal in the 200 to 400 Hz frequency band is attributed mostly to "direct" combustion noise, which has the travel time of the acoustic wave in the combustor and turbine. Beyond the turbine both direct and indirect pressure signals travel at the speed of an acoustic wave to the far field. Consequently, this source separation method identifies in the turbofan engine direct combustion noise and indirect combustion noise due to hot spots convecting through the turbine.

Nomenclature

B_e	resolution bandwidth, Hz, $B_e = 1/T_d = r/NP = 16$ Hz
D	propagation time delay or Lag, sec
f	frequency, Hz

f_c upper frequency limit, $f_c = 1/2\Delta t = r/2$, Hz (32 768 Hz)
$G_{xx}(f)$ auto power spectral density function defined for non-negative frequencies only (one-sided)
$G_{xy}(f)$ cross power spectral density function defined for non-negative frequencies only (one-sided)
$h(\tau)$ weighting function
$H(f)$ transfer function frequency response
$h(\tau)$ weighting function or unit impulse response function
L_y number of frequencies, $f_c/\Delta f = N/2$ (2048)
N segment length, number of data points per segment (4096)
N_s number of disjoint (independent) data segments/blocks, $N_s = B_e T_{total} = 1120$
P P-percent confidence interval
r sample rate, samples/sec (65 536)
$s_c(t)$ combustor input signal
$s_F(t)$ far-field output signal
T_{total} total record length, sec ($\approx$ 70 sec)
$T_d(i)$ record length of segment i, N/r, 0.0625 sec
$W_{s_F s_F}(f)$ coherent output power spectral function

Subscripts

i running segment index
$K(t)$ combustor pressure transducer sensor signal
$M(t)$ far-field microphone signal
$n(t)$ signal noise
$x(t)$ signal x
$y(t)$ signal y

Symbols

Δf frquency step, $1/T_d$, Hz (16 Hz)
Δt sampling interval, $1/r$ (1/65 536) sec
$\gamma^2_{nn}(f)$ magnitude squared noise coherence, 0.00267
$\gamma^2_{xy}(f)$ magnitude squared coherence (MSC) function
$\theta_{xy}(f)$ cross-spectrum phase angle

I. Introduction

The National Aeronautics and Space Administration (NASA) Aeronautics program is involved in creating noise reduction technology, which is an improvement over the 1997 state-of-the-art noise reduction technology. NASA is completing engine test programs to identify dominant noise sources. Core noise is of interest since it might become a significant contributor to the overall turbofan engine noise during takeoff or approach when the fan and jet noise are reduced because of forward velocity effects. In addition, future advances in fan and jet noise reduction technologies may cause core noise to be a more significant contributor to the overall turbofan engine noise.

The data analyzed is from a Honeywell TECH977 dual spool, turbofan engine. The engine is similar to the TECH7000, which is a development version of the Honeywell HTF7000 engine that currently powers the Challenger 300 aircraft. The test was conducted as part of the NASA/Honeywell Engine Validation of Noise and Emissions Reduction Technology (EVNERT) program. The particular set of test data was collected to test source separation procedures as part of a team effort with the Georgia Tech Research Institute. Consequently, in addition to eight far-field microphones signals from one pressure transducer in the combustor, two pressure transducers in the Low Pressure Turbine Exit, and two pressure transducers in the bypass duct were available.

The results presented are based on coherence function calculations using the far-field microphone and the combustor pressure transducer. Similar coherence function analysis was used starting 30 years ago to evaluate core noise from several engines. The following examples come to mind: an AVCO Lycoming YF–102 by Karchmer and Reshotko (1976),[1] Karchmer (1977),[2] Reshotko et al. (1977),[3] and Krejsa (1987);[4] an APU by Shivashankara (1978);[5] the General Electric CF6–50 by Doyle and Moore (1980);[6] the Pratt & Whitney JT15D by Reshotko and Karchmer (1980);[7] and the Pratt & Whitney JT9D by Shivashankara (1983).[8] In the same time period, the coherence function between a combustor pressure sensor and a far-field

microphone was measured for a gas turbine combustor using a single fuel spray nozzle assembly taken from a Boeing 502–7D gas turbine unit by Strahle et al. (1977)[9] and Muthukrishnan et al. (1978)[10] in studies of turbofan engine core noise.

Recently similar coherence function analysis techniques were used to evaluate core noise from a Pratt & Whitney PW4098 by Miles (2006).[11] The data evaluated was acquired from a test conducted as part of the NASA Engine Validation of Noise Reduction Concepts (EVNRC) Program in 2001. In the time interval between these two sets of tests, that is, from 1980 to 2000, turbofan engines have changed with newer engines such as the Pratt & Whitney PW4098 and the Honeywell TECH977 being based on new materials and a longer history of experience in turbofan manufacturing, design, analysis, and optimization. In evaluating the PW4098 core noise data, it was found that one consequence of these design changes is that the coherent part of the core noise signal has decreased.[11] In order to evaluate small coherence function values, a new diagnostic tool using aligned and unaligned coherence functions was developed. This tool which is explained by Miles[11] also needs to be applied to signals acquired in this Honeywell TECH977 test program since the core noise coherence values are small.

Core noise of a Rolls-Royce BR700 aero-engine has also been studied with the aid of a phased linear array of microphones by Siller et al. (2001)[12] and a combustor pressure sensor. Coherence between the combustor pressure sensor and a phased-array signal was obtained and the coherent array output power spectrum was measured.

One source of turbofan engine combustion noise is attributed to an unsteady combustion process, which produces unsteady pressures that propagate through the turbine to the far field. This is known as "direct" combustion noise mechanism. The relation between heat release and pressure waves was studied by Chu (1955).[13] Strahle (1971)[14] developed a framework that explained past experimental studies of direct combustion generated noise from flames using an approach similar to the one Lighthill (1952, 1954)[15,16] used in his studies of aerodynamic noise. Further developments in scaling laws were derived by Strahle (1972, 1975)[17,18] involving the first Eulerian time derivative of the chemical reaction rate integrated over the reacting volume. A review of current theories of scaling laws is given by Strahle (1975).[19] The study of combustion generated noise from turbulent flames is a continuing area of research. For example, the spectral characteristics of premixed flame noise has been studied by Rajaram (2003, 2006)[20,21] and large eddy simulation computations to predict combustion-generated noise in nonpremixed turbulent jet flames have been conducted by Ihme et al. (2006).[22] Thermoacoustic sources and instabilities are discussed by Dowling (1992).[23]

Another source of turbofan engine combustion noise is known as the "indirect" mechanism in which the noise is generated in the turbine by the interaction of entropy fluctuations ("hot spots") from the combustion chamber. This indirect source was studied by Pickett (1975),[24] Cumpsty and Marble (1977),[25,26] Cumpsty (1979),[27] and Gliebe (2000).[28] The indirect mechanism also functions when an entropy fluctuation interacts with an area change as shown by Cuadra (1967)[29] or a nonuniform flow as shown by Goldstein (1979)[30] and when an entropy or density nonuniformity is convected through a nozzle as shown by Williams and Howe (1970)[31] and Marble and Candel (1977).[32]

Strahle et al. (1977)[9] investigate direct combustion noise from an isolated combustor and discuss the problem of the mixture of "pseudosound" and sound in a combustor. The coherent combustion noise is discussed and the presence of incoherent noise is noted. Coherence between pressure measurements in the can combustor and far-field microphones are discussed and analyzed using a combustion acoustic model. Muthukrishnan et al. (1978)[33] discuss tests using a nozzle attached to the combustor can. The importance of direct noise and indirect noise (noise from hot spots passing through area changes and gradients) is discussed. Without the nozzle when no pressure drop occurred downstream of the combustor, the far-field noise was due to a direct combustion noise mechanism. When the flow was accelerated by the nozzle the indirect combustion noise mechanism appeared dominant.

Miles et al. (1983)[34] measured the cross spectra between temperature and pressure in a constant area duct downstream of a combustor and showed that the entropy fluctuations (hot spots) moved with the flow speed. Schemel et al. (2004)[35] studied experimentally and numerically entropy noise generated by hot spots (from a combustor) passing through a nozzle. Richter et al. (2005)[36] studied the application of computational aeroacoustic methods to indirect combustion noise generated by hot spots passing through a nozzle. Bake et al. (2005)[37] studied experimentally and numerically indirect combustion noise generated by hot spots (from a combustor) passing through a nozzle and verified that the entropy fluctuations (hot spots) moved with the flow speed. Bake et al. (2007)[38] studied experimentally indirect combustion noise

generated by hot spots (created by electrical heating) passing through a nozzle and verified that the entropy fluctuations (hot spots) moved with the flow speed.

The net travel time of the indirect combustion noise signal from the combustor to the far field is increased since the travel velocity of the hot spots to the turbine and in the turbine is the flow velocity. This flow velocity is some small fraction of the speed of sound. Miles et al. (1983)[34] has shown the pressure and entropy should be in phase in the combustor. Consequently, one might expect that the pressure signal from an indirect combustion noise source would be delayed relative to a pressure signal from a direct combustion noise source since an indirect combustion noise signal does not travel with the speed of an acoustic wave until it interacts with the turbine. Miles shows herein that the cross-spectra is a tool that provides a way to measure this time delay. Using this tool direct and indirect coherent combustion noise can be separated.

II. Coherent Output Power Spectrum

In the past, methods have been developed using spectrum analysis techniques to characterize acoustic signals from different sources mixed with noise. Bendat and Piersol (1966, 1971, 1980)[39–41] discuss these methods. Among the methods discussed is one using coherent output power spectra for noise source identification. The application of this technique that is of interest is the use of coherent output power spectra to separate and identify correlated combustion noise in far-field measurements of turbofan engine noise. Karchmer (1977)[2] and Karchmer et al. (1977)[42] use the coherence function calculated from internal microphone measurements of fluctuating pressures in the combustor and far-field acoustic pressures to determine the correlated combustion noise of a YF102 turbofan engine at far-field locations by calculating the coherent output power spectrum. A typical results showed the coherence measured between the combustor pressure and the 120^o far-field acoustic pressure had a roughly Gaussian-shaped distribution in the range 0 to 200 Hz with a peak near 125 Hz and a maximum value at 30 percent fan speed of 0.38 and at 43 percent fan speed a maximum value of 0.5 (Ref. 2, Figs. 39 and 48). The corresponding combustion coherence output power spectrum for the 43 percent fan speed case has a peak near 125 Hertz and a generally domelike shape. The peak is about $20\log(0.5) = -6.02$ dB below the peak of the far-field spectrum at 120 Hz. The dome edges are 20 dB down at 40 Hz and 200 Hz.

The basic formulation for the coherent output power spectrum is presented by Bendat and Piersol (1980).[41] We assume that the far-field output signal, s_F, is the output of a constant parameter linear system with weighting function $h(\tau)$ and frequency response $H(f)$. The output of the system is given by the convolution integral of the combustor input signal, $s_c(t)$

$$s_F(t) = \int_0^\infty h(\tau) s_c(t-\tau) d\tau \tag{1}$$

Then, the far-field combustion noise spectrum, $G_{s_F s_F}(f)$, and the combustion noise cross spectrum between the far-field signal and the combustor pressure sensor signal, $G_{s_F s_c}(f)$ are related to the combustor pressure sensor signal as follows:

$$G_{s_F s_F}(f) = \mid H(f) \mid^2 G_{s_c s_c}(f) \tag{2}$$

$$G_{s_F s_c}(f) = H(f) G_{s_c s_c}(f) \tag{3}$$

Here the cross-power spectrum between the combustor pressure sensor signal, $x(t)$, and the far-field microphone signal, $y(t)$, is $\hat{G}_{xy}(f)$ and the corresponding combustor pressure sensor power spectra and far-field spectra are $\hat{G}_{xx}(f)$ and $\hat{G}_{yy}(f)$.

$$\hat{G}_{xx}(f) = \hat{G}_{s_c s_c}(f) + \hat{G}_{n_1 n_1}(f) \tag{4}$$

$$\hat{G}_{yy}(f) = \hat{G}_{s_F s_F}(f) + \hat{G}_{n_2 n_2}(f) \tag{5}$$

These are obtained by averaging many (approx. 2000) successive directly calculated power spectral densities using a 70 second total observation time, a sampling rate of $2^{16} = 65\,536$ samples per second; and a 50 percent overlap in the spectrum calculations. In practice, only estimates, $\hat{G}_{xy}(f)$ of $G_{xy}(f)$, $\hat{G}_{xx}(f)$ of $G_{xx}(f)$, and $\hat{G}_{yy}(f)$ of $G_{yy}(f)$ can be obtained due to the finite observation interval and the $\hat{}$ notation will be dropped.

The combustion noise reaching a microphone will be estimated using the magnitude squared coherence function, $\gamma^2_{xy}(f)$, where

$$\gamma^2_{xy}(f) = \frac{\mid G_{xy}(f) \mid^2}{G_{xx}(f)G_{yy}(f)} \tag{6}$$

Then

$$\mid G_{xy}(f) \mid^2 = \mid G_{s_F s_c}(f) \mid^2 = \mid H(f) \mid^2 G^2_{s_c s_c}(f) = G_{s_F s_F}(f)G_{s_c s_c}(f) \tag{7}$$

and the coherent output power spectrum, $W_{s_F s_F}(f)$, is

$$\begin{aligned} W_{s_F s_F}(f) &= \gamma^2_{xy}(f)G_{yy}(f) \\ &= G_{s_F s_F}(f)\frac{G_{s_c s_c}(f)}{G_{s_c s_c}(f) + G_{n_1 n_1}(f)} \end{aligned} \tag{8}$$

where we assume the extraneous noise terms are uncorrelated with each other and with the signals.

$$G_{s_c n_1}(f) = G_{s_F n_2}(f) = G_{n_1 n_2}(f) = 0 \tag{9}$$

The quantity $W_{s_F s_F}(f)$ can also be called the coherent combustion noise spectrum. Thus, the estimated coherent output power spectrum, $W_{s_F s_F}(f) = \gamma^2_{xy}(f)G_{yy}(f)$, will determine $G_{s_F s_F}(f)$ when the input noise is zero, $G_{n_1 n_1}(f) = 0$, regardless of the output noise $G_{n_2 n_2}(f)$. In the frequency range of interest, we may assume $G_{n_1 n_1}(f) = 0$ or just consider that $W_{s_F s_F}(f)$ is a measure of the coherent combustion noise.

III. Sensors, Arena Layout, and Signal Processing

Internal engine sensor locations are shown in Fig. 1. The test was conducted at the San Tan acoustic cell 966 on March 23, 2006, with a "L-shaped" barrier minimizing inlet noise radiation to the aft microphones. As shown in Figs. 2 and 3 the short leg of the barrier is perpendicular to the nozzle, with this piece starting a few feet upstream of the nozzle exit. In addition, this piece does not reach the nozzle but stops a few feet away from the nozzle. The long leg of the barrier sweeps along parallel to the engine ending forward of the Inflow Control Device (ICD).

The ICD that prevents turbulent stretched vortex structures from interacting with the fan is shown in Fig. 3. The engine condition power settings discussed are 48, 54, and 60 percent of the Max Power setting. Microphone locations used in the test program are shown in Fig. 4. For this test, external microphones were at 10^o, 30^o, 50^o, 70^o, 90^o, 110^o, 130^o, and 160^o measured from the inlet. The signal estimation parameters used are shown in Table 1.

The test was conducted when the air temperature was about 9 ^{o}C (48 ^{o}F) and the microphone radius was 30.48 m. The engine is at a height of 3.048 m. Consequently, with a speed of sound of 337 m/sec, the travel time for a signal to leave the combustor and reach a microphone is about 90.44 ms (5927 samples). This will be called the measured time delay herein. Using the analysis parameters shown in Table 1, the segment length, $T_d = 1/16$ is 62.5 ms (4096 samples). Consequently, if one calculates the coherence of the combustor pressure transducer signal, $K(t)$ and a microphone signal $M(t)$ using the measured time histories as measured one finds the coherence is that of random noise since the two signals are totally independent except at frequencies where tones are present as discussed by Miles (2006).[11] This is due to the fact that the origin of the two signals does not overlap in the signal processing interval specified by the segment length, T_d. The noise coherence confidence interval value is approximately given by

$$\gamma^2_{nn} = \gamma^2_{KM}(f, D > T_d) = 1 - (1 - P)^{1/(N_s - 1)} \tag{10}$$

where this formula determines a P-percent confidence interval. Thus the 95-percent confidence interval noise floor is $\gamma^2_{nn} = 0.00267$ ($N_s = 1120$).

To align the two signals, the far-field microphone signal can be adjusted by moving it backward using a time delay of $D = 0.09044 * 65\ 536 = 5927$ samples based on the signal propagation time. Using computer code a new aligned array of time history values can be created for each microphone signal. This new array will then be more in phase with the combustor pressure transducer signal. In Fortran the computer code statements that create the new time history is

```
do j=1,Total_number_of_samples
M_aligned(j)=M_unaligned(j+5927)
enddo
```

This code slides the points beyond point 5927 backward to align with the K(t) sequence of points thereby removing the time delay.

This approach does not take into account a multiplicity of reasons why this travel time delay calculated from the speed of sound and microphone radius might not be best. For example, the center of the 100 foot microphone radius might not correspond to the origin of the sound. In addition, no wind gradient or temperature profiles are used though they might be important in some cases. A discussion on how one can use spherical decay to account for engine noise component source locations is given by Salikluddin et al. (2006).[43]

A slightly more sophisticated procedure to obtain the alignment time D was used herein. The correct time delay makes the cross-spectrum phase angle change with frequency minimal in the range of maximum coherence. Consequently, cross-spectrum phase angles were calculated using correction time delay D values in the range of 1000 to 9000 in 100 count steps. From these cross-spectrum phase angle plots the best value of D was selected based on the criterion that the variation of the phase angle with frequency will have a gradient of zero when the time histories are aligned. Again, this value is also the value of D that maximizes the coherence in the frequency range of interest. In some cases when using this procedure, an increase in coherence of 15 to 27 percent was noted over the use of a universal D value based on travel time calculated using the measured microphone radius and a speed of sound based on the air temperature.

Table 2 shows the signals measured. The combustor pressure transducer signal is on Channel 9 (CIP1). Channels 10 and 11 measure pressures downstream of the turbine (T551 and T552). Channels 12 and 13 measure bypass duct pressures (BPD1 and BPD2).

IV. Phase Angle Standard Deviation

The coherence function is especially important since the cross-spectrum phase angle, $\theta_{xy}(f)$, standard deviation can be related to the coherence function. In Bendat (1980)[41] and in Piersol (1981)[44] the random error in the phase estimates due to statistical sampling is given in terms of the standard deviation of the estimated phase angle, $\overline{\theta}_{xy}(f)$, by

$$\sigma\left[\overline{\theta}_{xy}(f)\right] \approx \sin^{-1}\left\{\frac{\left[1-\gamma_{xy}^2(f)\right]^{1/2}}{|\gamma_{xy}|\sqrt{2N_s}}\right\} \tag{11}$$

where $\sigma\left[\overline{\theta}_{xy}(f)\right]$ is measured in radians and as used herein N_s is selected to be the number of segments or blocks used in the spectral calculations. For the special case where the term in curly brackets is small Eq. 11 becomes

$$\sigma\left[\overline{\theta}(f)\right] \approx \frac{\left[1-\gamma_{xy}^2(f)\right]^{1/2}}{|\gamma_{xy}|\sqrt{2N_s}} \tag{12}$$

where for the unknown coherence $\gamma_{xy}^2(f)$ the estimated coherence $\overline{\gamma}_{xy}^2(f)$ is used. A plot of the standard deviation of the phase angle in degrees versus coherence is shown in Fig. 5 for $N_s = 234, 468, 1120$, and 2240. When the coherence is 0.003, Fig. 5 shows the pressure sensor cross-spectrum phase angle standard deviation should be between 15^o and 25^o. Only phase angles with coherence values greater than 0.003 will be shown in the cross-spectrum phase angle plots.

V. Results

Results are presented in groups arranged by engine speed. Figures 6 through 13 present the 48 percent speed case, figures 14 through 21 present the 54 percent speed case, and figures 22 through 29 present the 60 percent speed case. Within each engine speed group the results are arranged by angle. Each figure consists of a set of four plots. Figure (a) shows the aligned coherence on a linear scale so that the results are more readily compared with previous results. Figure (b) shows the coherence on a logarithmic scale so that the aligned and unaligned coherence and the statistical noise floor coherence, $\gamma_{nn}^2 = 0.00267$ ($N_s = 1120$),

can be clearly revealed. Figure (c) shows the cross-spectrum phase angle. Figure (d) shows the SPL density and the coherent combustion noise spectral density calculated using the aligned and unaligned coherence, and the statistical coherence of two unaligned signals.

On each figure the signal propagation value of D which was used is shown in counts and seconds. The D values are also shown in Table 3. While the nominal value is 5927 samples, larger D values are used at the smaller angles and smaller values are used at the larger angles.

A. Coherence

For each engine speed case the aligned and unaligned coherence values are shown. In addition, the noise floor coherence value of $\gamma^2_{nn} = 0.00267$ is shown. The coherence is largest in the 0 to 400 Hz frequency range. The aft quadrant coherence function is generally in the vicinity of 0.2 or lower. The improved coherent output power spectrum method is needed to determine the coherent combustion noise spectrum due to its low level.

To illustrate the sensitivity of selection of the time delay, D, we note that to remove the gradient of the phase angle versus frequency in the frequency range from 0 to 200 Hz shown for the 130^o microphone in Figs. 12, 20, and 28 for the 48, 54, and 60 percent of the Max Power setting, the time delay used is $D = 5900/65\ 536 = 90.027$ ms. However, to remove the gradient of the phase angle versus frequency in the frequency range from 200 to 400 Hz shown for the 130^o microphone in Figs. 30, 31, and 32 at the three power settings, the time delay used is $D = 5700/65\ 536 = 86.975$ ms. This indicates that the noise in the 200 to 400 Hz frequency band has traveled faster by a factor of $5900/5700 = 1.035$ than the noise in the 0 to 200 frequency band. The actual values of the coherence and the two signal coherent output power spectrum do not change much since the signal alignment using either time delay is fine.

Miles (1983)[45] has shown that the acoustic pressure and temperature fluctuations are related and that the cross-spectrum shows phase angle depends mainly on the slowest propagation speed which is that of the hot spot in the flow. Consequently, on the basis of the time delay ($D = 5900/65\ 536 = 90.027$ ms) used to remove cross-spectrum phase angle changes with frequency, we make the argument that below 200 Hz the coherence is due mainly to an indirect combustion noise process due to entropy waves, which spend part of the time traveling at the flow velocity (in the combustor). Also, again on the basis of the time delay ($D = 5700/65\ 536 = 86.975$ ms) used to remove cross-spectrum phase angle changes with frequency in the 200 to 400 Hz band, this coherence is due mainly to a direct combustion noise source, which spends all its time propagating as an acoustic wave with the velocity of an acoustic wave.

Similar behavior was identified at the 110^o microphone where the indirect (entropy) noise signal time was 93.079 ms and the direct (acoustic) noise signal travel time was 90.027 ms. Furthermore, similar behavior was also identified at the 160^o microphone where the indirect (entropy) noise signal time was 85.449 ms and the direct (acoustic) noise signal travel time was 82.397 ms.

It is likely that the measured coherence represents in reality, a combination of direct and indirect noise sources and that some time delay, which is a function of frequency should be used to remove the cross-spectrum phase angle changes. However, that investigation is beyond the scope of this report. Since, the time delays are the result of a combination of sources without a detailed source acoustic and propagation model, detailed geometry and detailed performance information it difficult to assign precise velocities and lengths to obtain these time delay values.

Muthukrishnan et al. (1978)[33] make a similar argument that at low-frequencies a high coherence exists between combustion noise and entropy noise. However, they argue that at moderate frequencies the phase becomes rapidly oscillatory which destroys the coherence and makes the entropy noise and combustion noise independent, uncorrelated sources. Consequently, the combustor pressure at low-frequencies is coherent with entropy noise. At higher frequencies it is coherent with direct combustion noise.

In any event, the cross spectra between the combustion sensor pressure and the far-field microphone pressure provides some indication that the time delay before the indirect mechanism changes a hot spot into an acoustic wave can be estimated and direct and indirect coherent combustion noise can be separated.

B. Tones in the coherence

As discussed by Miles (2006)[11] tones can be identified using the aligned and unaligned coherence function. The unaligned coherence function has a value determined by the number of samples of two independent signals and the tones. The aligned signal has a value determined by the coherence of the

two signals and tones. For the engine condition power setting of 48 percent a strong tone occurs at 352 Hz. Aligned and unaligned coherence values for this case are shown in Table 4. For the engine condition power setting of 54 percent a strong tone occurs at 368 Hz. Aligned and unaligned coherence values for this case are shown in Table 5. For the engine condition power setting of 60 percent a strong tone occurs at 384 Hz. Aligned and unaligned coherence values for this case are shown in Table 6. These tones generally can be related to a shaft frequency. The physical N2 shaft rotation rates are 21 340, 22 310, and 22 930 rpm, which correspond to shaft frequencies of 355.667, 371.83, and 382 Hz. Since the bandwidth being used is 16 Hz the observed tones correspond to the physical N2 shaft frequency. Consequently, these appear to be compressor tones possibly related to a compressor disk tone. For the engine condition power setting of 60 percent for the 10^o microphone a strong tone not only occurs at 384 Hz but also at the second harmonic, 768 Hz.

C. Cross-spectrum phase angle

If the coherence is larger than 0.003 the phase angle standard deviation with $N_s > 2000$ is between 15^o and 25^o (see Fig. 5). Consequently, the phase angle plots emphasize measured phase angles where the coherence is greater than 0.003.

The phase angle plots measured at angles greater than 90^o for coherence values greater than 0.003 show a smooth profile. However, for angles less than 90^o the profile of the phase angles is more ragged even though the coherence is greater than 0.003. This might indicate the barrier is creating an interference pattern that shows up in the coherent low-frequency sound waves. Consequently, the best values of the phase angle are in the aft arc at angles greater than 90^o.

VI. Discussion

The correlated far-field core noise component from the Honeywell TECH977 covers the frequency range from 0 to 400 Hz. Similar results were obtained by Miles (2006)[11] in the study of a Pratt & Whitney PW4098 turbofan engine, by Siller et al.(2001)[12] in the study of core noise from a Rolls-Royce BR700 aero-engine, and in the study of an AVCO Lycoming YF–102 by Karchmer and Reshotko (1976),[1] and Karchmer (1977).[2] Karchmer (1983)[46] in the study of AVCO Lycoming YF–102 core noise and Miles (2006)[11] in the study of core noise from a Pratt & Whitney PW4098 attribute this coherent noise to the lowest radial order modes of the combustion noise. The lowest radial order mode is the $m = 0$ mode, which corresponds to a plane wave. Karchmer (1983)[46] used six pressure probes to identify combustor modes. Miles (2007)[47] used a restricted acoustic model analysis using signals from two combustor pressure sensors to identify combustor modes.

The turbofan combustor is designed to have a high level of turbulence without being unstable. As far back as 1957, Blackshear and Rayle (1957)[48] mention that some observers report beneficial effects due to velocity and pressure excursions evidenced in a noticeable increase in the combustion efficiency within the combustor. Poinsot and Veynante (2005)[49] (see p. 131) remark that the main effect of turbulence on combustion is to increase the combustion rate. Hill and Peterson (1992)[50] mention that more intense turbulence promotes more rapid mixing of the vaporized fuel and air and faster propagation of flame through the unburned mixture. They present a good discussion of gas turbine combustor fundamental design issues.

The coherence measurements in turbofan engines between the combustor and the far-field microphones differ from those made using a combustor burner assembly with a single fuel spray nozzle as used by Strahle et al. (1977)[9] and Muthukrishnan et al. (1978)[10] due to the presence of the fan inlet sound source, the fan exhaust sound source, the jet sound source, and the engine core sound source. The coherence measurements in turbofan engines are influenced by the fact that turbofan engine have an annular combustor with the circumferential modes. In addition, the coherence measurements, should reflect the possibility of entropy noise from hot spots passing through the turbine as discussed by Pickett (1975),[24] Cumpsty and Marble (1977),[25] and Gliebe (2000),[28] as well as direct combustion noise and compressor tones. However, coherence measurements made using a combustor burner assembly with a single fuel spray nozzle as used by Strahle et al. (1977)[9] and Muthukrishnan et al. (1978)[10] do have a jet noise source and the possibility of entropy noise from hot spots passing through a nozzle as described by Williams and Howe (1970)[31] and Marble and Candel (1977).[32]

Table 7 shows that for a great number of combustion chamber geometries, range of the number of nozzles, and engine design bypass ratios significant coherence can be measured from 120^o to 160^o. The

combustion duct modal analysis of Karchmer (1983)[46] and Miles (2007)[47] suggest that the coherence is due to annular combustion duct modes propagating to the far field and at the lowest frequencies the coherence is from a plane wave combustion duct mode. The interesting aspect is that one sees any coherence at all considering each fuel nozzle is an independent source of noise and the level of turbulence used to increase combustor efficiency and reduce emissions is high.

For many engines the coherence in the far field is less than 0.1 and one may use the method of aligned and unaligned coherence developed by Miles (2006)[11] to determine if the coherence is significant. Note, for example, that for the CF6–50 core noise investigation described by Doyle and Moore (1980)[6] the number of samples was 100, and the 95 percent confidence interval for coherence of two independent signals using 100 samples is zero to $\gamma_{nn}^2 = 1 - (1 - 0.95)^{1/(100-1)} = 0.0298$. Doyle and Moore (1980)[6] plotted coherence values on a linear scale from 0 to 1.0, and coherence values less than 0.1 were ignored. To some extent the coherence value of 0.1 has traditionally been considered a threshold or "cutoff" level of coherence. The discussion presented herein shows that this is not a realistic value for modern turbofan engines.

At first glance the behavior of the barrier seems to block the low-frequency jet mixing noise thereby increasing the combustion noise coherence in the forward quadrant. However, the barrier should also be blocking the combustion noise. It appears that the barrier creates some type of reflection channel that changes the path of both signals to the forward quadrant microphones. Furthermore, the results presented herein show that by manipulating the delay time, D, one can enhance the combustion noise signal perhaps by picking up more reflections and reduce the low-frequency jet mixing noise signal. Consequently, the forward quadrant microphone results especially at the 48 percent maximum power test condition are highly manipulated. At higher power setting, the coherence levels resemble those in the aft arc and are not modified by the barrier as much.

The peak coherence values summarized in Table 8 suggest that one of the major noise source reducing the coherence between the combustor and the far-field microphones as shown in Table 7 is low-frequency noise from near the end of the potential core of the jet. Phase array measurements of jet noise show that a distributed source of low-frequency noise near the end of the potential core of the jet. The peak locations of the source levels gradually move from downstream positions to the nozzle exit as the frequency is increased as shown by phased array measurements made by Lee and Bridges (2005),[51] Lee (2006),[52] Papamoschou and Dadvar (2006),[53] and Suzuki (2006).[54] The low-frequency generating mechanism is attributed to large-scale vortical structure collapse at the end of the potential core. At an engine speed of 48 percent of maximum power, the jet is shorter and weaker than at the higher speeds. The reflecting channel formed by the barrier wall and the selected signal time delay may be reducing the ratio of low-frequency jet noise to combustion-related low-frequency noise so that the coherence is high at angles of 30^o, 50^o, and 70^o at the 48 percent speed operating condition. As the engine power is increased to 54 and 60 percent the potential core of the jet moves further downstream reducing the effectiveness of the barrier to interact with the low-frequency noise generated near the end of the potential core and the low-frequency combustion noise becomes weaker. Consequently, the coherence values and angular distribution are both more similar to those in the literature at the higher engine power settings. The effect of the jet on combustor coherence was noted by Muthukrshnam et al. (1978)[10] in a test of a single fuel spray nozzle combustor assembly. A similar effect of the jet on the coherence function between a microphone array focused on the nozzle and a rumble probe is discussed for tests of a BR700 engine by Siller et al. (2001).[12] Since much of the low-frequency noise appears to come from jet mixing at the end of the jet potential core, using acoustic liners in the turbofan nozzle exhaust system to remove core noise will not remove much low-frequency noise except at low engine speed settings where the jet noise is reduced.

The sound radiation spectrum of flames is a topic of current experimental research by Rajaram et al. (2004, 2006)[21, 55] and computational fluid dynamic research using the large-eddy simulation technique by Ihme et al. (2006).[22] In addition, research to study the interaction of sound and flames is being conducted by Lieuwen and Cho (2005)[56] and the effect of noise on combustion stability is being studied by Lieuwen and Banaszuk (2005).[57] However, there is a gap between these studies of the acoustics of a flame from a fuel spray nozzle and the acoustical interaction of multiple fuel spray combustor nozzles in an annular combustor. The mechanism leading to the formulation of annular acoustic duct modes from the sound generated multiple independent fuel spray nozzles is unknown. The amount of the total sound energy participating in the annular duct modes is unknown. If only part of the total sound energy is measured by the coherence function from the combustor to the far field, then the remainder will show up in the far field as radiated sound unattributable to the combustor noise. Perhaps the annular acoustic duct modes represent a steady-state phenomena as

sound energy is added by the multiple spray combustor nozzles and removed as sound leaves the combustor. At the moment the ratio of uncorrelated sound to coherent sound in the combustor duct is an open question.

VII. Concluding Remarks

The source location technique based on adjusting the time delay between the combustor pressure sensor signal and the far-field microphone signal to maximize the coherence and remove as much variation of the phase angle with frequency as possible was successful. A method to help identify combustion noise coherence using an aligned and unaligned coherence technique, which enables the validation of low levels of coherence as being due to core noise by identifying the coherence noise floor has been demonstrated. A statistical procedure was also used to establish this threshold level. The use of both methods provides a high confidence level for the coherence function values calculated.

Using the procedures discussed led to the discovery that the turbofan engine noise in the 200 to 400 Hz frequency band is chiefly related to coherent "direct" combustion noise, which travels from the combustor to the far field as an acoustic signal. Furthermore, it was found that the noise signal in the 0 to 200 Hz frequency band is chiefly related to coherent "indirect" combustion noise due to "hot spots" traveling through the turbine, which travel at the flow velocity in the combustor and turbine until noise is generated.

For the AVCO Lycoming YF–102 the coherence between the combustor and a far-field microphone was frequently near 0.5. For the Pratt & Whitney PW4098 this coherence was generally less than 0.1. For the 48 percent of maximum power test condition the far-field coherence was generally less than 0.4 at angles from 90^o to 160^o. At angles greater than 90^o for operating settings of 54 and 60 percent, the coherence between the combustor and a far-field microphone is less than 0.15.

References

[1]Karchmer, A. M. and Reshotko, M., "Core Noise Source Diagnostics on a Turbofan Engine Using Correlation and Coherence Techniques," Tech. Rep. NASA TMX-73535, NASA, 1976.

[2]Karchmer, A. M., "Identification and Measurement of Combustion Noise From a Turbofan Engine Using Correlation and Coherence Techniques," Tech. Rep. NASA TM-73747, NASA, 1977, Doctor of Philosophy thesis E-9319.

[3]Reshotko, M., Karchmer, A., Penko, P. F., and McArdle, J. G., "Core Noise Measurements on a YF–102 Turbofan Engine," *J. Aircraft*, Vol. **14** No. 7, July 1977, pp. 611–612, NASA TM X-73587, AIAA Paper 77-21.

[4]Krejsa, E. A., "Combustion Noise From Gas Turbine Aircraft Engines Measurement of Far-Field Levels," Tech. Rep. NASA-TM-88971, 1987.

[5]Shivashankara, B. N., "Gas Turbine Core Noise Source Isolation by Internal-to-Far-Field Correlations," *J. Aircraft*, Vol. **15** No. 9, September 1978, pp. 597–600.

[6]Doyle, V. L. and Moore, M. T., "Core Noise Investigation of the CF6–50 Turbofan Engine," Tech. Rep. R79AEG395, NASA CR-159598, General Electric Company, Cincinnati, OH, Jan. 1980, Contract-Grant-Task Number: NAS3-21260.

[7]Reshotko, M. and Karchmer, A., "Core Noise Measurements From a Small, General Aviation Turbofan Engine," Tech. Rep. TM-81610, NASA, 1980, N81-11769.

[8]Shivashankara, B. N., "High Bypass Ratio Engine Noise Component Separation by Coherence Technique," *J. Aircraft*, Vol. **20** No. 3, March 1983, pp. 236–242, AIAA 81-2054, Aeroacoustics Conference, 7th, Palo Alto, California, Oct. 5-7, 1981.

[9]Strahle, W. C., Muthukrishnan, M., and Neale, D. H., "Coherence Between Internal and External Noise Generated by a Gas Turbine Combustor," *AIAA Journal*, Vol. **15** No. 7, 1977, pp. 1018–1024, AIAA-1977-20; NASA NSG-3015.

[10]Muthukrishnan, M., Strahle, W. C., and Neale, D. H., "Separation of Hydrodynamic, Entropy, and Combustion Noise in a Gas Turbine Combustor," *AIAA Journal*, Vol. **16** No. 4, April 1978, pp. 320–327.

[11]Miles, J. H., "Aligned and Unaligned Coherence: A New Diagnostic Tool," Tech. Rep. AIAA-2006-0010, AIAA, 2006, Presented at the 44th AIAA Aerospace Science Meeting, 9-12 Jan 2006 Reno Hilton Reno, Nevada, also NASA/TM–2006-214112.

[12]Siller, H. A., Arnold, F., and Michel, U., "Investigation of Aero-Engine Core-Noise Using a Phased Microphone Array," Tech. Rep. AIAA-2001-2269, AIAA/CEAS Aeroacoustics Conference, 2001.

[13]Chu, B.-T., "Pressure Waves Generated by Addition of Heat in a Gaseous Medium," Tech. Rep. NACA TN 3411, NACA, 1955.

[14]Strahle, W. C., "On Combustion Generated Noise," *Journal of Fluid Mechanics*, Vol. **49** , 1971, pp. 399–414.

[15]Lighthill, M. J., "On Sound Generated Aerodynamically : I. General Theory." *Proceedings of the Royal Society London*, Vol. **211** Series A, 1952, pp. 564–587.

[16]Lighthill, M. J., "On Sound Generated Aerodynamically: II. Turbulence as a Source of Sound," *Proceedings of the Royal Society London*, Vol. **222** Series A, Feb. 1954, pp. 1–32.

[17]Strahle, W. C., "Some Results in Combustion Generated Noise," *Journal of Sound and Vibration*, Vol. **23** No. 1, 1972, pp. 113–125.

[18]Strahle, W. C. and Shivashankara, B. N., "A Rational Correlation of Combustion Noise Results From Open Turbulent Premixed Flames," *Fifteenth Symposium (International) on Combustion*, The Combustion Institute, Pittsburgh, 1975, pp. 1379–1385.

[19]Strahle, W. C., "The Convergence of Theory and Experiment in Direct Combustion Generated Noise," AIAA-1975-522, March 1975, NASA grant NSG-3015; AF-AFOSR-72-2385.

[20]Rajaram, R. and Lieuwen, T., "Parametric Studies of Acoustic Radiation From Premixed Flames," *Combustion Science and Technology*, Vol. **175** No. 12, December 2003, pp. 2269–2298.

[21]Rajaram, R., Gray, J., and Lieuwen, T., "Premixed Combustion Noise Scaling: Total Power and Spectra," AIAA-2006-2612, May 2006.

[22]Ihme, M., Bodony, D. J., and Pitsch, H., "Prediction of Combustion-Generated Noise in Non-premixed Turbulent Jet Flames Using Large-Eddy Simulation," Tech. Rep. AIAA 2006-2614, AIAA, May 2006.

[23]Crighton, D. G., Dowling, A. P., Williams, J. F., Heckel, M., and Leppington, F., *Modern Methods in Analytical Acoustics: Lecture Notes*, Springer-Verlag, 1992.

[24]Pickett, G. F., "Core Engine Noise Due to Temperature Fluctuating Through Turbine Blade Rows," Tech. Rep. AIAA-75-528, AIAA, 1975.

[25]Cumpsty, N. A. and Marble, F. E., "The Interaction of Entropy Fluctuations With Turbine Blade Rows; A Mechanism of Turbojet Noise." *Proc. R. Soc. Lond. A.*, Vol. **357**, 1977, pp. 323–344.

[26]Cumpsty, N. A. and Marble, F., "Core Noise from Gas Turbine Exhausts," *Journal of Sound and Vibration*, Vol. **54** No. 2, 1977, pp. 297–309.

[27]Cumpsty, N. A., "Jet Engine Combustion Noise: Pressure, Entropy and Vorticity Perturbations Produced by Unsteady Combustion or Heat Addition," *Journal of Sound and Vibration*, Vol. **66** No. 4, 1979, pp. 527–544.

[28]Gliebe, P., Mani, R., Shin, H., Mitchell, B., Ashford, G., Salamah, S., and Connell, S., "Acoustic Prediction Codes," Tech. Rep. NASA CR–2000-210244, R99AEB169, General Electric Aircraft Engines, August 2000.

[29]Cuadra, E., "Acoustic Wave Generation by Entropy Discontinuities Flowing Past an Area Change," *J. Acoust. Soc. Am.*, Vol. **42** No. 4, 1967, pp. 725–732.

[30]Goldstein, M. E., "Turbulence Generated by the Interaction of Entropy Fluctuations With Non-Uniform Mean Flows," *J. Fluid Mech.*, Vol. **93** Part 2, 1979, pp. 209–224.

[31]Williams, J. E. F. and Howe, M. S., "The Generation of Sound by Density Inhomogeneities in Low Mach Number Nozzle Nlow," *J. Fluid Mech.*, Vol. **70** Part 3, 1970, pp. 605–622.

[32]Marble, F. E. and Candel, S. M., "Acoustic Disturbance From Gas Non-Uniformities Convected Through a Nozzle," *Journal of Sound and Vibration*, Vol. **55** No. 2, 1977, pp. 225–243.

[33]Muthukrishnan, M., Strahle, W. C., and Neale, D. H., "Separation of Hydrodynamic, Entropy, and Combustion Noise in a Gas Turbine Combustor," *AIAA Journal*, Vol. **16** No. 4, April 1978, pp. 320–327, NASA NSG 3015.

[34]Miles, J. H., Wasserbauer, C. A., and Krejsa, E. A., "Cross Spectra Between Temperature and Pressure in a Constant Area Duct Downstream of a Combustor," AIAA-83-0762, NASA TM-83351, 1983.

[35]Schemel, C., Thiele, F., Bake, F., Lehmann, B., and Michel, U., "Sound Generation in the Outlet Section of Gas Turbine Combustion Chambers," AIAA-2004-2929, 2004.

[36]Richter, C., Panek, L., and Thiele, F. H., "On the Application of CAA-Methods for the Simulation of Indirect Combustion Noise," AIAA-2005-2919, May 2005.

[37]Bake, F., Michel, U., Rohle, I., Richter, C., Thiele, F., Liu, M., and Noll, B., "Indirect Combustion Noise Generation in Gas Turbines," AIAA-2005-2830, May 2005.

[38]Bake, F., Michel, U., and Roehle, I., "Investigation of Entropy Noise in Aero-Engine Combustors," *Transactions of the ASME Journal of Engineering for Gas Turbines and Power*, Vol. **129**, April 2007, pp. 370–376.

[39]Bendat, J. S. and Piersol, A. G., *Measurement and Analysis of Random Data*, John Wiley & Sons, 1966.

[40]Bendat, J. S. and Piersol, A. G., *Random Data: Analysis and Measurement Procedures*, John Wiley & Sons, 1971.

[41]Bendat, J. S. and Piersol, A. G., *Engineering Applications of Correlation and Spectral Analysis*, John Wiley & Sons, 1980.

[42]Karchmer, A., Reshotko, M., and Montegani, F., "Measurement of Far Field Combustion Noise From a Turbofan Engine Using Coherence Functions," Tech. Rep. AIAA Paper 77-1277, NASA, Oct. 1977, NASA TM-73748, N77-33163.

[43]Salikuddin, M., Stimpert, D., and Majjigi, R., "A Method to Account for Engine Noise Component Source Locations," Tech. Rep. AIAA 2006-2554, 12th AIAA/CEAS Aeroacoustics Conference (27th AIAA Aeroacoustics Conference) 8-10 May 2006, Cambridge, Massachusetts, 2006.

[44]Piersol, A., "Time Delay Estimation Using Phase Data," *IEEE Transactions on Acoustics, Speech, and Signal Processing*, Vol. **ASSP-29** No. 3, June 1981, pp. 471–477.

[45]Miles, J. H., Wasserbauer, C. A., and Krejsa, E., "Cross Spectra Between Temperature and Pressure in a Constant Area Duct Downstream of a Combustor," AIAA-83-0762, NASA TM-83351, 1983.

[46]Karchmer, A. M., "Acoustic Modal Analysis of a Full Scale Annular Combustor," Tech. Rep. AIAA Paper 83-0760, NASA, 1983, NASA TM-83334.

[47]Miles, J. H., "Restricted Modal Analysis Applied to Internal Annular Combustor Auto-Spectra and Cross-Spectra Measurements," *AIAA Journal*, Vol. **45** No. 5, May 2007, pp. 968–999.

[48]Blackshear, P. L. and Rayle, W. D., "Oscillations in Combustors," *Basic Considerations in the Combustion of Hydrocarbon Fuels With Air*, edited by H. C. Barnett and R. R. Hibbard, NACA-TR-1300 **VIII**, NACA, 1957, pp. 229–241.

[49]Poinsot, T. and Veynante, D., *Theoretical and Numerical Combustion*, R. T. Edwards, 2005.

[50]Hill, P. G. and Peterson, C. R., *Mechanics and Thermodynamics of Propulsion*, Addison Wesley, 1992.

[51]Lee, S. S. and Bridges, J., "Phased-Array Measurements of Single Flow Hot Jets," Tech. Rep. AIAA 2005-2842, 11th AIAA/CEAS Aeroacoustics Conference (26th AIAA Aeroacoustics Conference) 23 - 25 May 2005, Monterey, California, 2005.

[52]Lee, S. S., "Phased-Array Measurements of Modern Regional Aircraft Turbofan Engine Noise," Tech. Rep. AIAA 2006-2653, 12th AIAA/CEAS Aeroacoustics Conference (27th AIAA Aeroacoustics Conference) 8-10 May 2006, Cambridge, Massachusetts, 2006.

[53]Papamoschou, D. and Dadvar, A., "Localization of Multipel Types of Jet Noise Sources," Tech. Rep. AIAA 2006-2644, 12th AIAA/CEAS Aeroacoustics Conference (27th AIAA Aeroacoustics Conference) 8-10 May 2006, Cambridge, Massachusetts, 2006.

[54]Suzuki, T., "Coherent Noise Radiation From a Jet Investigated With a Beam-Forming Technique," Tech. Rep. AIAA 2006-2646, 12th AIAA/CEAS Aeroacoustics Conference (27th AIAA Aeroacoustics Conference) 8-10 May 2006, Cambridge, Massachusetts, 2006.

[55]Rajaram, R. and Lieuwen, T., "Effect of Approach Flow Turbulence Characteristics on Sound Generation From Premixed Flames," Tech. Rep. AIAA 2004-461, 42nd AIAA Aerospace Sciences Meeting and Exhibit 5-8 January 2004, Reno, Nevada, 2004.

[56]Lieuwen, T. and Cho, J. H., "Coherent Acoustic Wave Amplification/Damping by Wrinkled Wlames," *Journal of Sound and Vibration*, Vol. **279** , 2005, pp. 669–686.

[57]Lieuwen, T. and Banaszuk, A., "Background Noise Effects on Combustor Stability," *Journal of Propulsion and Power*, Vol. **21** No. 1, January-February 2005, pp. 25–31.

Table 1. Spectral estimate parameters

Parameter	Value
Segment length, i.e., data points per segment, N	4096
Sample rate, r, samples/second	65 536
Segment length, $T_d = N/r$, seconds	0.0625
Sampling interval, $\Delta t = 1/r$, seconds	1/65 536
Frequency step, $\Delta f = 1/T_d$, Hz	16.0
Upper frequency limit, $f_c = 1/2\Delta t = r/2$, Hz	32 768
Number of frequencies, $Ly = f_c/\Delta f = N/2$	2048
Propagation time delay/Lag (T=9 ^{o}C,r=30.48 m) $D = 5927/65\ 536$, seconds	0.09044
Number of independent samples, n_s	1120
Overlap	0.50
Sample length, seconds	70

Table 2. Channel signals

Channel	Signal [Polar angles from inlet]
1	Microphone 2 [10^o]
2	Microphone 6 [30^o]
3	Microphone 10 [50^o]
4	Microphone 14 [70^o]
5	Microphone 18 [90^o]
6	Microphone 22 [110^o]
7	Microphone 26 [130^o]
8	Microphone 32 [160^o]
9	CIP1
10	T551
11	T552
12	BPD1
13	BPD2
14	Raw N1 Speed

Table 3. Signal propagation time delay in counts

Microphone	Percent Max. Power		
Angle, Degrees	48	54	60
10	7800	7100	7100
30	7300	7200	7200
50	6800	6900	6900
70	6500	6600	6600
90	6300	6300	6300
110	6100	6100	6100
130	5900	5900	5900
160	5600	5600	5600

Table 4. Angular variation of aligned and unaligned coherence of tone at 352 Hz for TECH977 engine power condition setting of 48 percent

Location	Microphone Angle, Degrees	Aligned Coherence D (See Table 3)	Unaligned Coherence $D = 0$
2-9	30	0.027	0.0198
3-9	50	0.0094	0.0242
4-9	70	0.0239	0.0258
5-9	90	0.0520	0.0412
6-9	110	0.0471	0.0397
7-9	130	0.0101	0.0032
8-9	160	0.0216	0.0405

Table 5. Angular variation of aligned and unaligned coherence of tone at 368 Hz for TECH977 engine power condition setting of 54 percent

Location	Microphone Angle, Degrees	Aligned Coherence D (See Table 3)	Unaligned Coherence $D = 0$
1-9	10	0.0948	0.0856
2-9	30	0.0292	0.0237
3-9	50	0.0142	0.0077
4-9	70	0.0639	0.00663
5-9	90	0.1101	0.0917
6-9	110	0.0297	0.0161
7-9	130	0.0422	0.0036
8-9	160	0.0538	0.0592

Table 6. Angular variation of aligned and unaligned coherence of tone at 384 Hz for TECH977 engine power condition setting of 60 percent

Location	Microphone Angle, Degrees	Aligned Coherence D (See Table 3)	Unaligned Coherence $D = 0$
1-9	10	0.0308	0.0373
2-9	30	0.0120	0.0123
3-9	50	0.0008	0.0040
4-9	70	0.0018	0.0013
5-9	90	0.0466	0.0206
6-9	110	0.0275	0.0153
7-9	130	0.0116	0.0152
8-9	160	0.0062	0.0063

Table 7. Some engine specifications

Engine	Number of Fuel Nozzles	Nominal Bypass Ratio	Typical Max. Combustor/Core to Far-Field Coherence γ^2 at 120^o to 160^o
AVCO Lycoming YF102[1]	28	6:1	0.5
General Electric CF6-50[6]	30	4.4:1 (Takeoff)	0.1
The Pratt & Whitney JT15D[7]	12	3.3:1	0.5
Pratt & Whitney JT9D[8]	20	5:1	0.4
Pratt & Whitney PW4098[11]	24	5.8	0.1
Honeywell TECH977 (HTF7000)	16	4.2	0.35

Superscripts refer to references

Table 8. Typical peak combustor to far-field coherence, γ^2

Percent of	Angle							
Maximum Power	10^o	30^o	50^o	70^o	90^o	110^o	130^o	160^o
48	NA	0.65	0.64	0.46	0.2	0.3	0.35	0.2
54	0.2	0.25	0.14	0.13	0.15	0.15	0.15	0.1
60	0.2	0.20	0.1	0.10	0.085	0.085	0.10	0.08

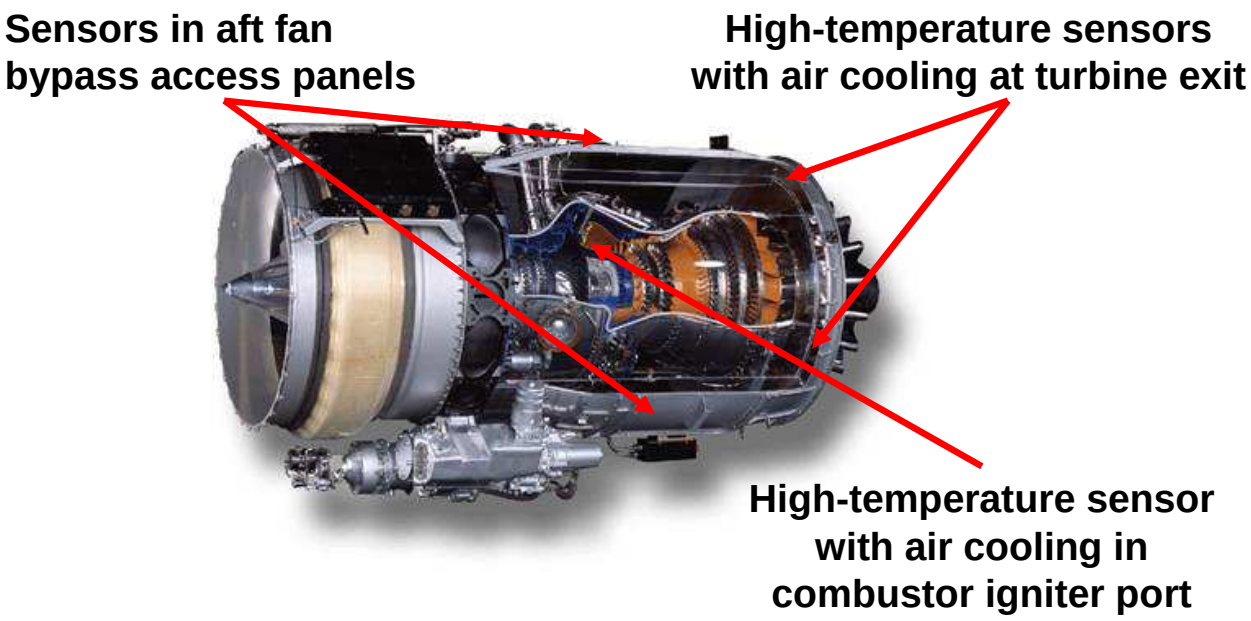

Figure 1. Engine internal sensor locations.

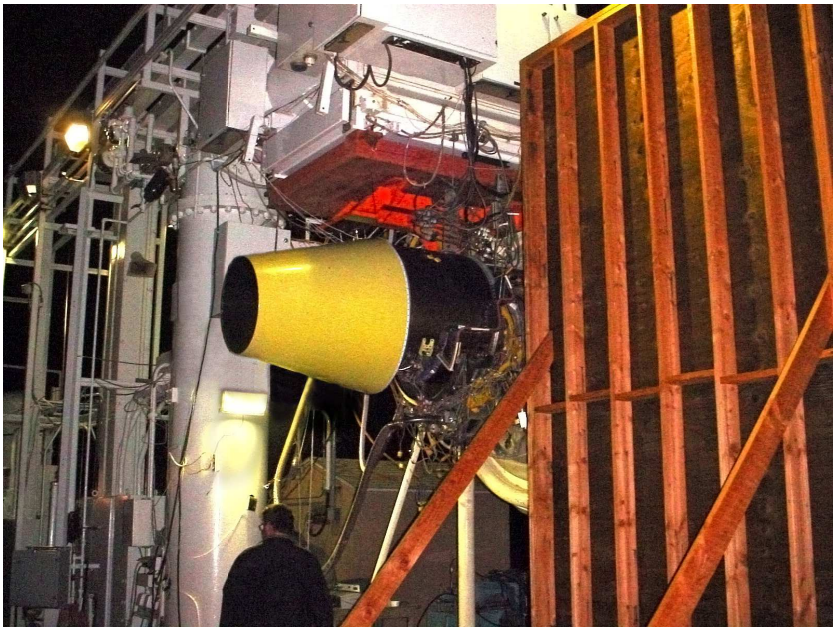

Figure 2. TECH977 with forward barrier from rear.

Figure 3. TECH977 with forward barrier from front.

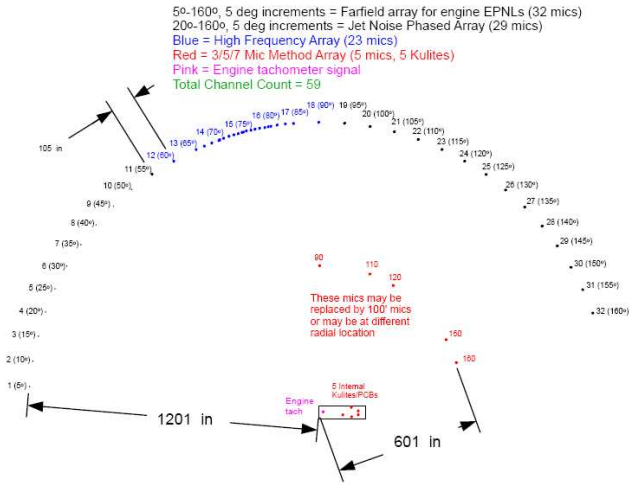

Figure 4. Microphone arrays used during test program.

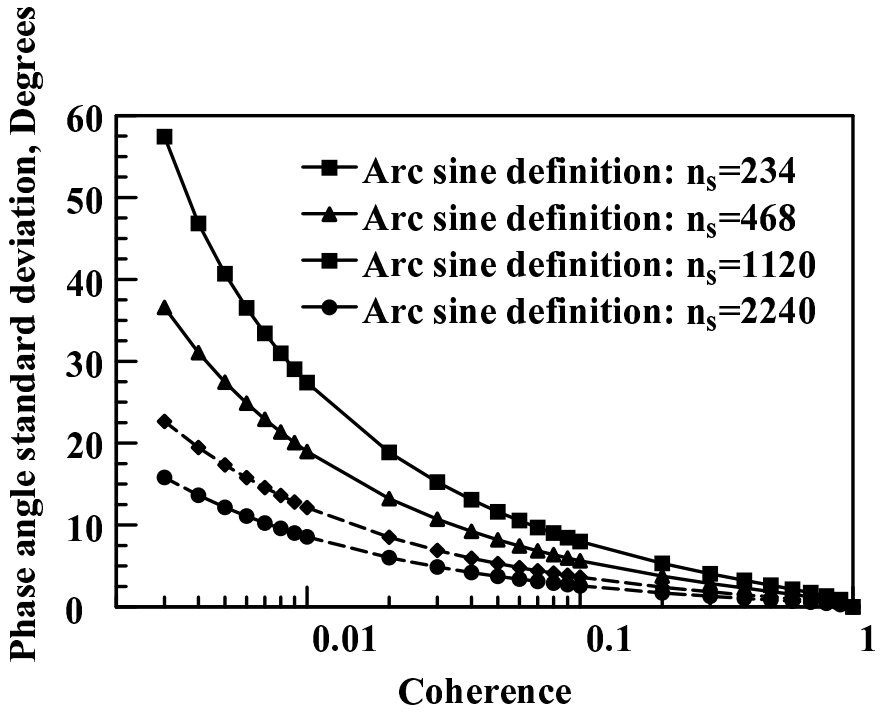

Figure 5. Standard deviation of G_{xy} phase angle as a function of γ_{xy}^2 for $n_s = 234$, 468, 1120, and 2240.

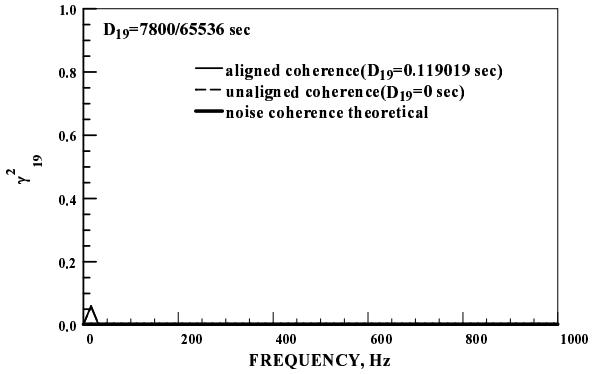

(a) Coherence between microphone at 10^o and C1P1 combustor pressure sensor.

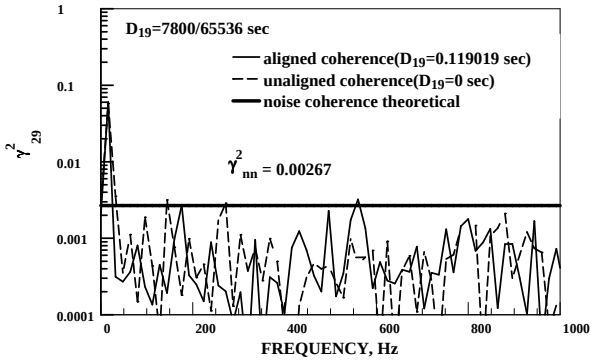

(b) Coherence between microphone at 10^o and C1P1 combustor pressure sensor.

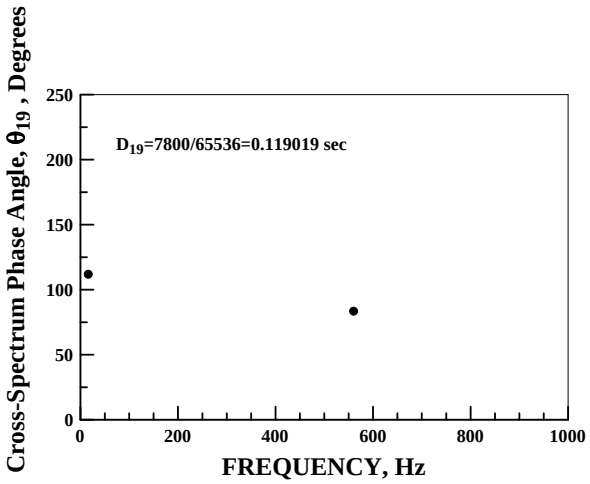

(c) Aligned cross-spectrum phase angle between microphone at 10^o and C1P1 combustor pressure sensor.

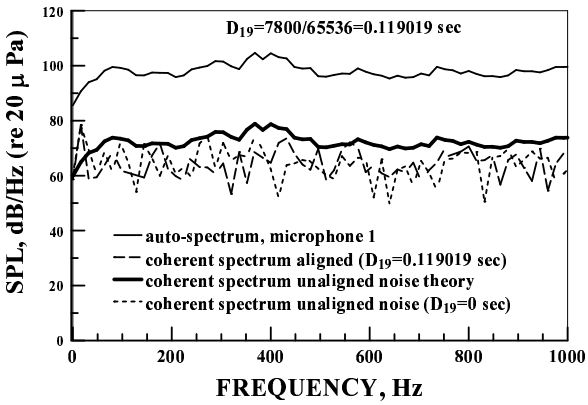

(d) Coherent output power at microphone at 10^o using C1P1 combustor pressure sensor.

Figure 6. TECH977 engine condition power setting of 48 percent microphone at 10^o.

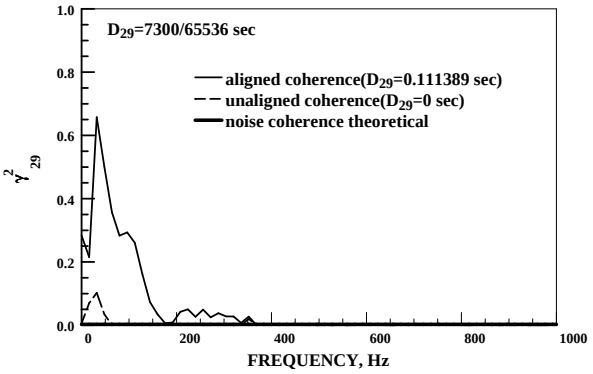

(a) Coherence between microphone at 30^o and C1P1 combustor pressure sensor.

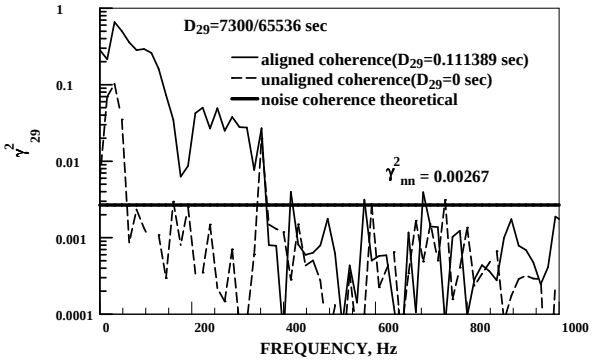

(b) Coherence between microphone at 30^o and C1P1 combustor pressure sensor.

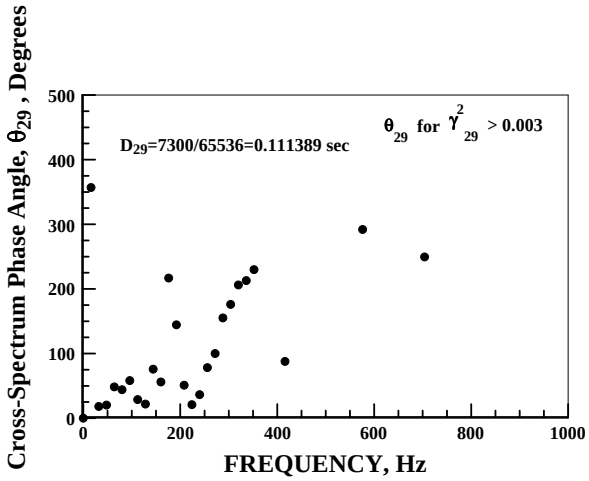

(c) Aligned cross-spectrum phase angle between microphone at 30^o and C1P1 combustor pressure sensor.

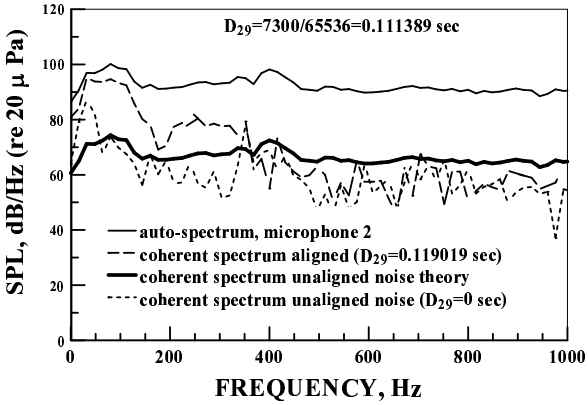

(d) Coherent output power at microphone at 30^o using C1P1 combustor pressure sensor.

Figure 7. TECH977 engine condition power setting of 48 percent microphone at 30^o.

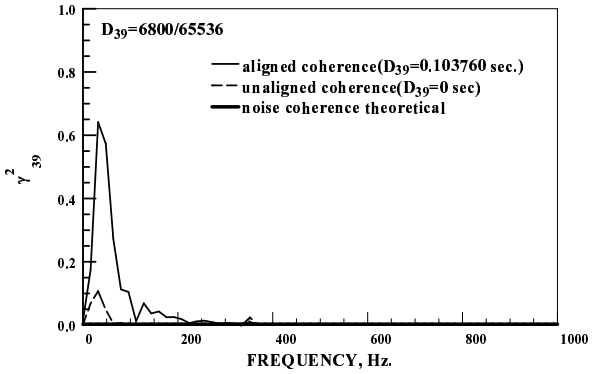

(a) Coherence between microphone at 50^o and C1P1 combustor pressure sensor.

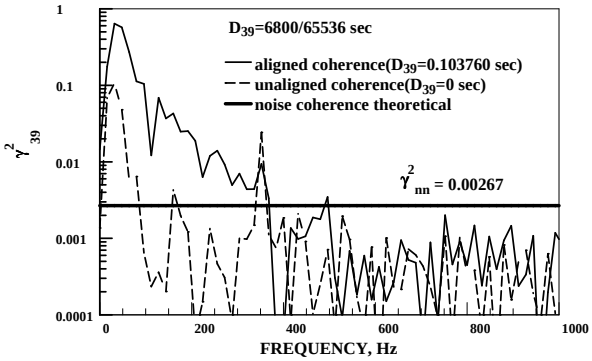

(b) Coherence between microphone at 50^o and C1P1 combustor pressure sensor.

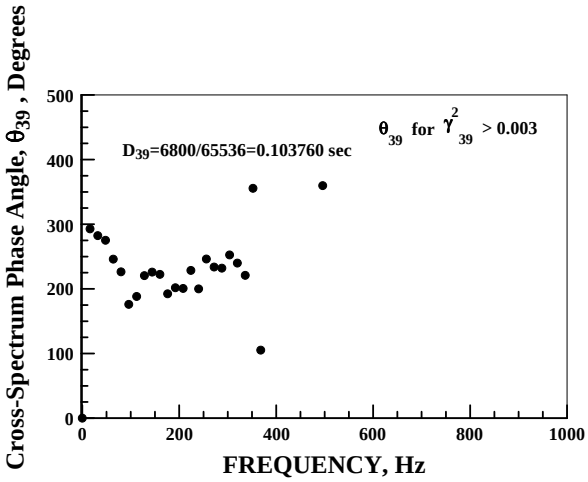

(c) Aligned cross-spectrum phase angle between microphone at 50^o and C1P1 combustor pressure sensor.

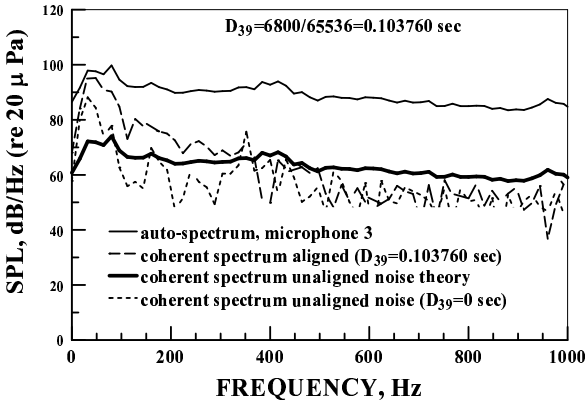

(d) Coherent output power at microphone at 50^o using C1P1 combustor pressure sensor.

Figure 8. TECH977 engine condition power setting of 48 percent microphone at 50^o.

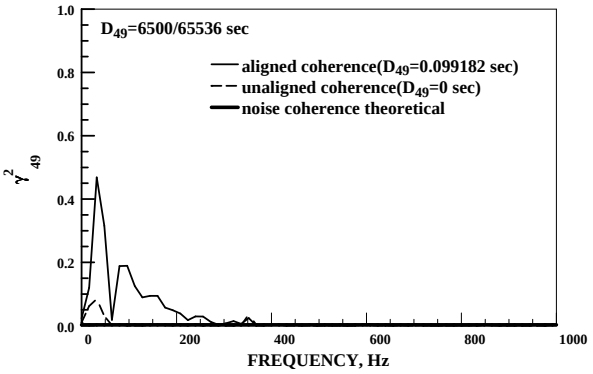

(a) Coherence between microphone at 70^o and C1P1 combustor pressure sensor.

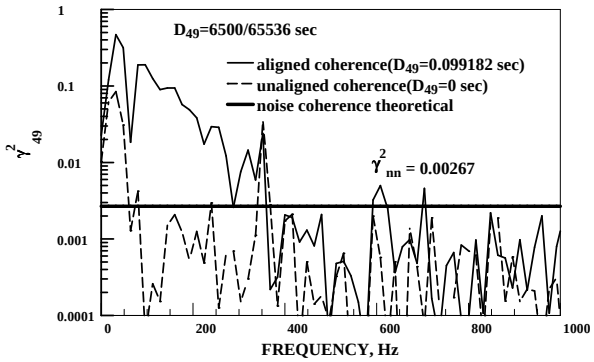

(b) Coherence between microphone at 70^o and C1P1 combustor pressure sensor.

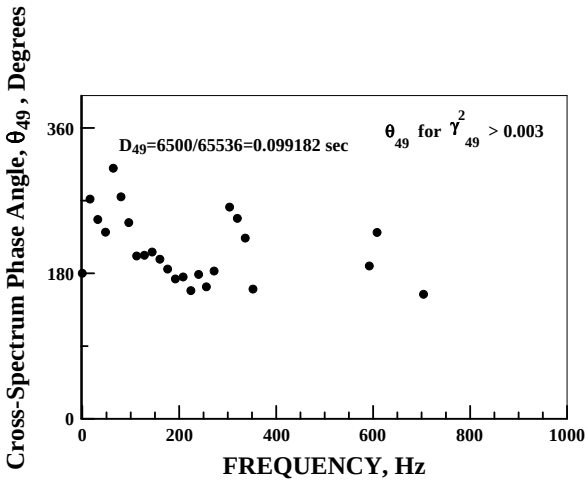

(c) Aligned cross-spectrum phase angle between microphone at 70^o and C1P1 combustor pressure sensor.

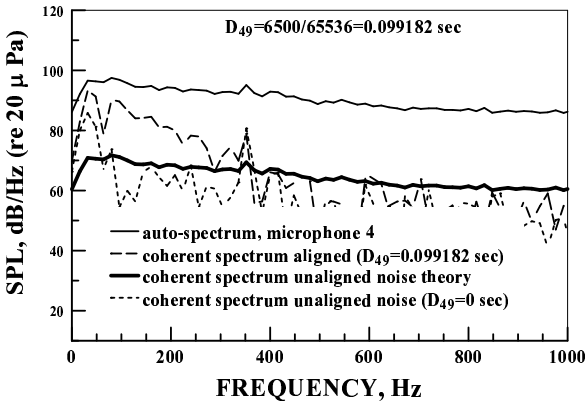

(d) Coherent output power at microphone at 70^o using C1P1 combustor pressure sensor.

Figure 9. TECH977 engine condition power setting of 48 percent microphone at 70^o.

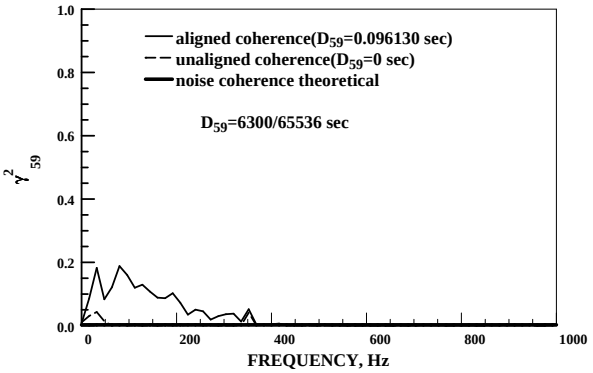

(a) Coherence between microphone at 90^o and C1P1 combustor pressure sensor.

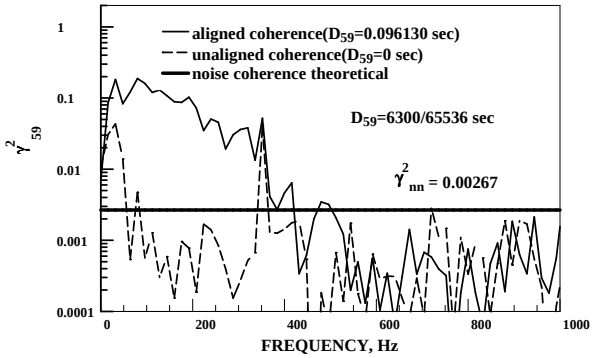

(b) Coherence between microphone at 90^o and C1P1 combustor pressure sensor.

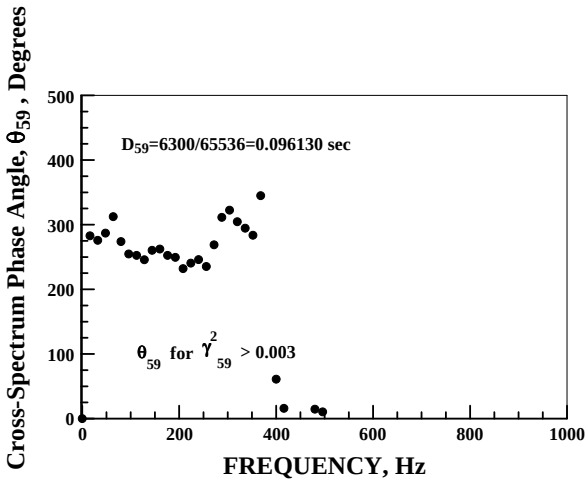

(c) Aligned cross-spectrum phase angle between microphone at 90^o and C1P1 combustor pressure sensor.

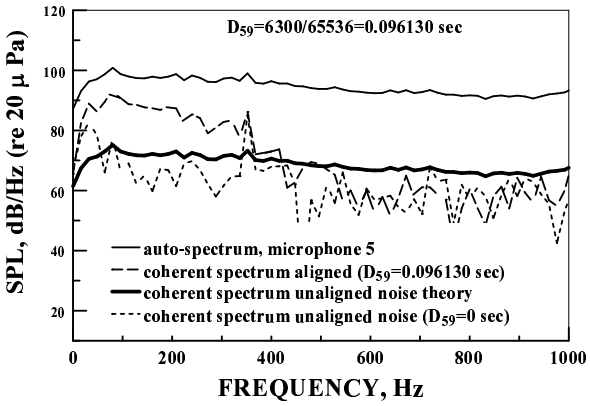

(d) Coherent output power at microphone at 90^o using C1P1 combustor pressure sensor.

Figure 10. TECH977 engine condition power setting of 48 percent microphone at 90^o.

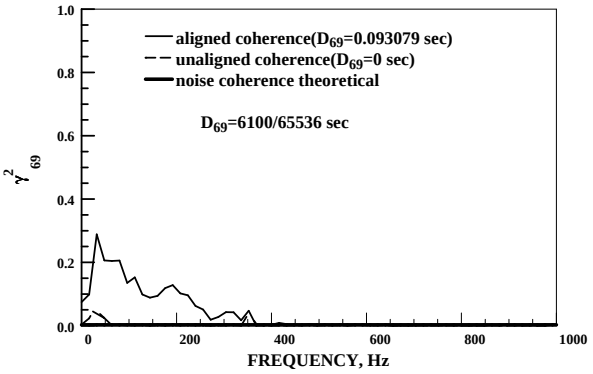

(a) Coherence between microphone at 110^o and C1P1 combustor pressure sensor.

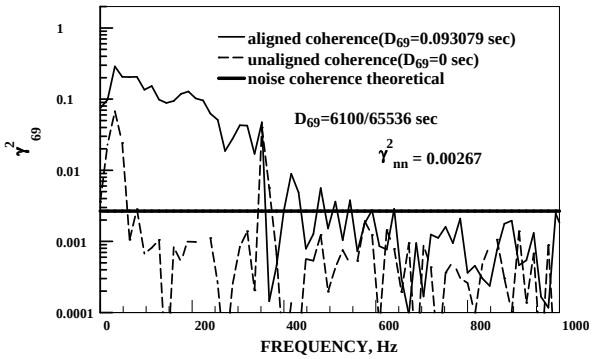

(b) Coherence between microphone at 110^o and C1P1 combustor pressure sensor.

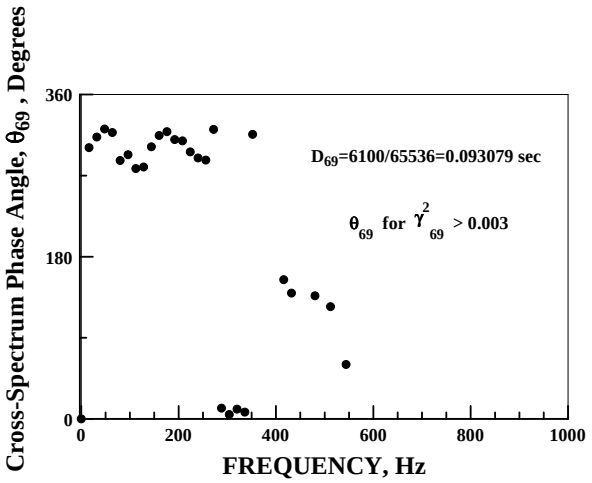

(c) Aligned cross-spectrum phase angle between microphone at 110^o and C1P1 combustor pressure sensor.

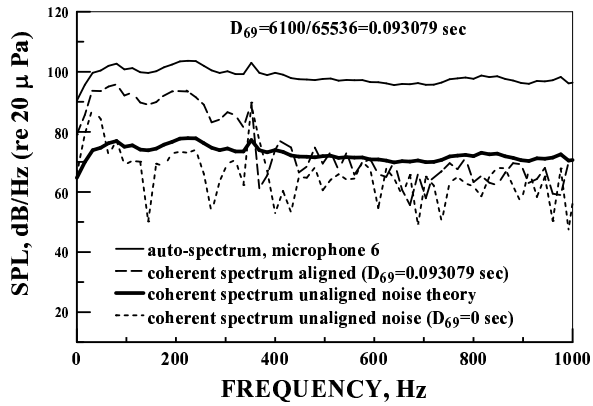

(d) Coherent output power at microphone at 110^o using C1P1 combustor pressure sensor.

Figure 11. TECH977 engine condition power setting of 48 percent microphone at 110^o.

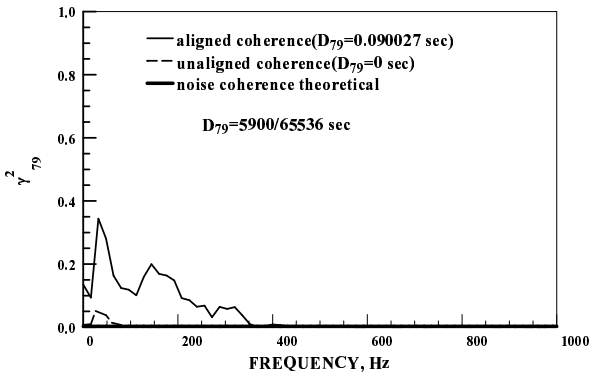

(a) Coherence between microphone at 130^o and C1P1 combustor pressure sensor.

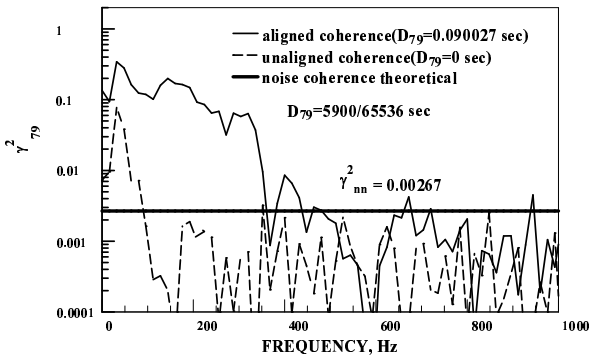

(b) Coherence between microphone at 130^o and C1P1 combustor pressure sensor.

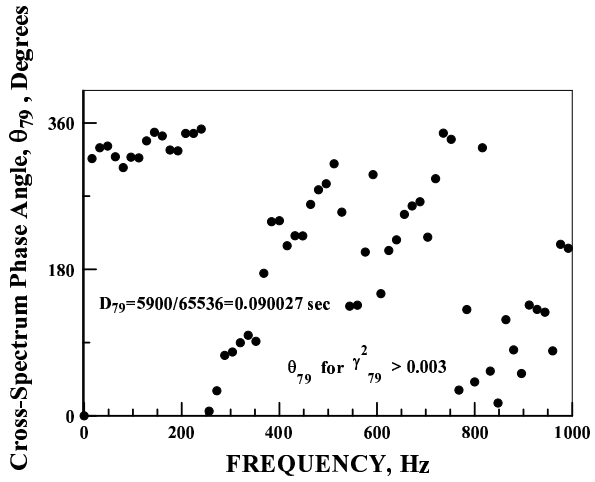

(c) Aligned cross-spectrum phase angle between microphone at 130^o and C1P1 combustor pressure sensor.

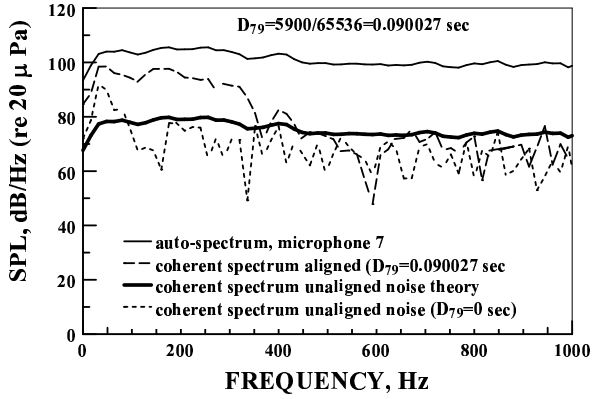

(d) Coherent output power at microphone at 130^o using C1P1 combustor pressure sensor.

Figure 12. TECH977 engine condition power setting of 48 percent microphone at 130^o.

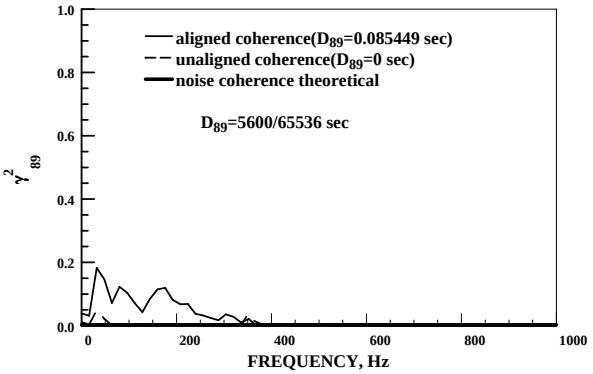

(a) Coherence between microphone at 160^o and C1P1 combustor pressure sensor.

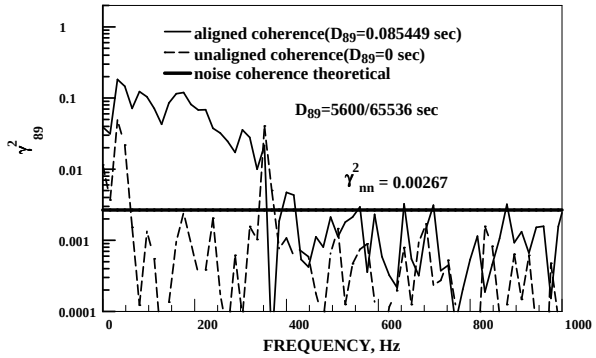

(b) Coherence between microphone at 160^o and C1P1 combustor pressure sensor.

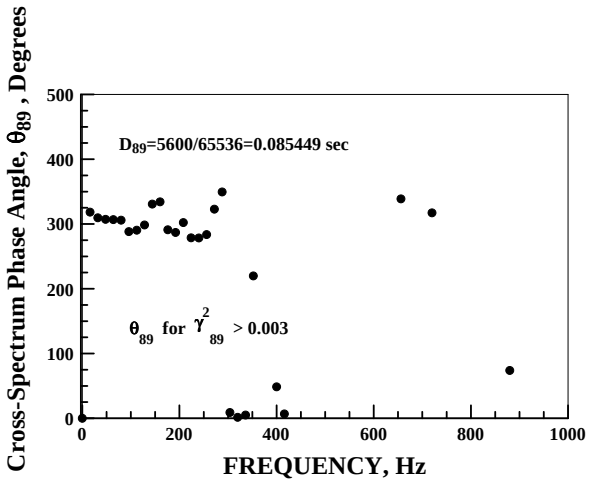

(c) Aligned cross-spectrum phase angle between microphone at 160^o and C1P1 combustor pressure sensor.

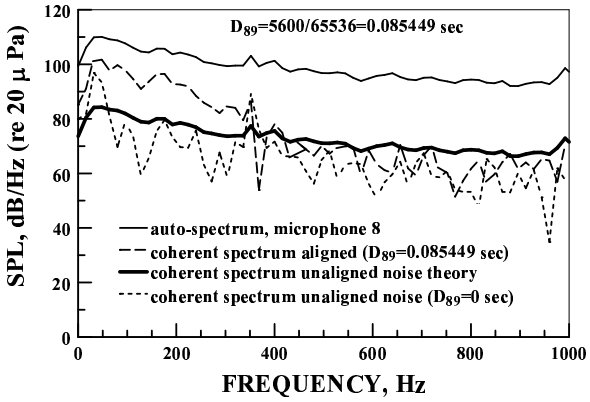

(d) Coherent output power at microphone at 160^o using C1P1 combustor pressure sensor.

Figure 13. TECH977 engine condition power setting of 48 percent microphone at 160^o**.**

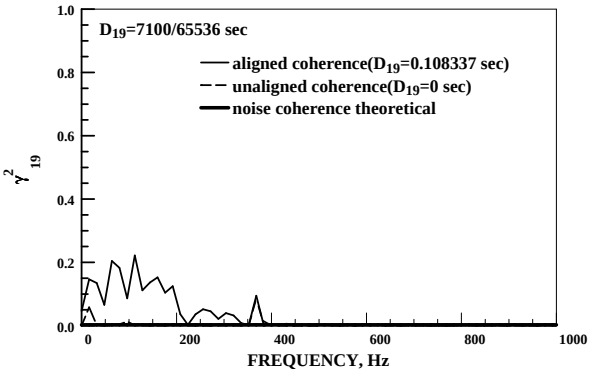

(a) Coherence between microphone at 10^o and combustor pressure sensor, C1P1.

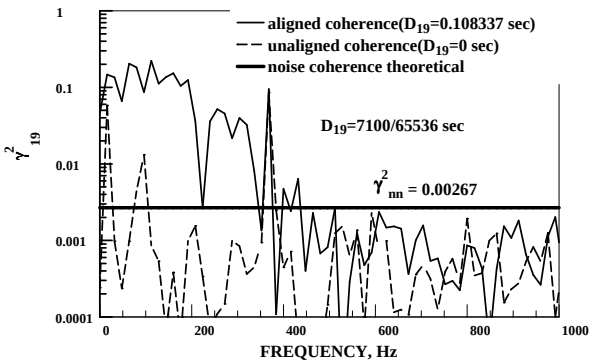

(b) Coherence between microphone at 10^o and combustor pressure sensor, C1P1.

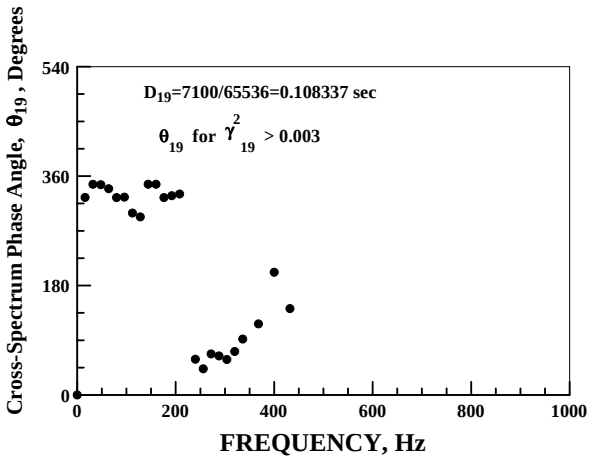

(c) Aligned cross-spectrum phase angle between microphone at 10^o and combustor pressure sensor, C1P1.

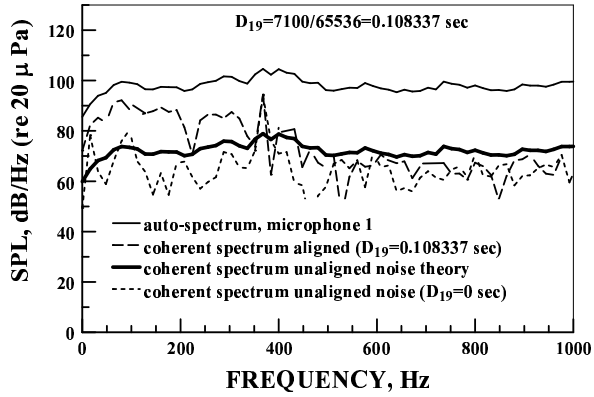

(d) Coherent output power at microphone at 10^o using combustor pressure sensor, C1P1.

Figure 14. TECH977 engine condition power setting of 54 percent microphone at 10^o.

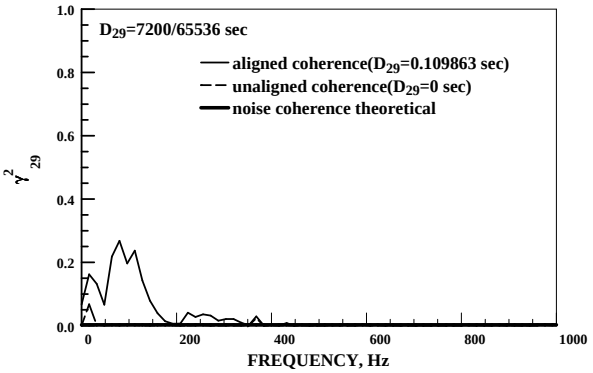

(a) Coherence between microphone at 30^o and combustor pressure sensor, C1P1.

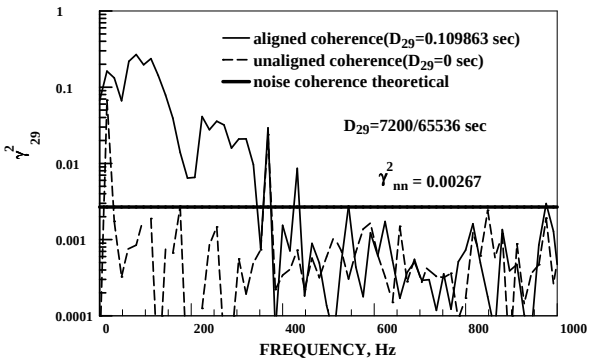

(b) Coherence between microphone at 30^o and combustor pressure sensor, C1P1.

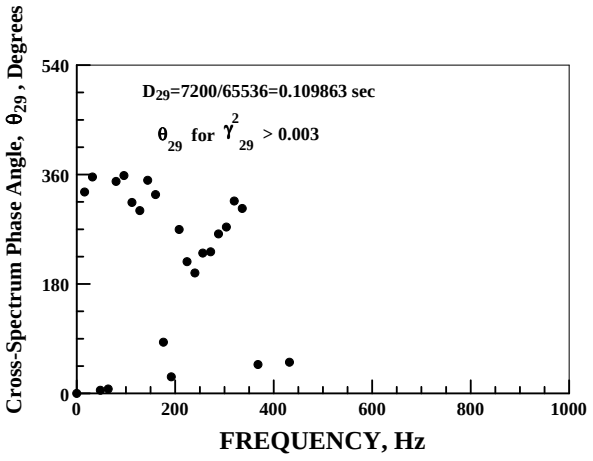

(c) Aligned cross-spectrum phase angle between microphone at 30^o and combustor pressure sensor, C1P1.

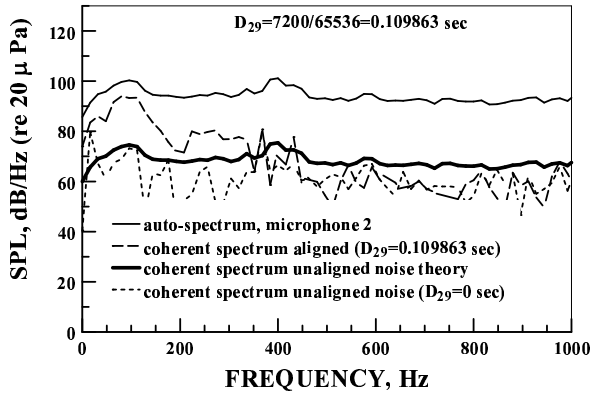

(d) Coherent output power at microphone at 30^o using combustor pressure sensor, C1P1.

Figure 15. TECH977 engine condition power setting of 54 percent microphone at 30^o.

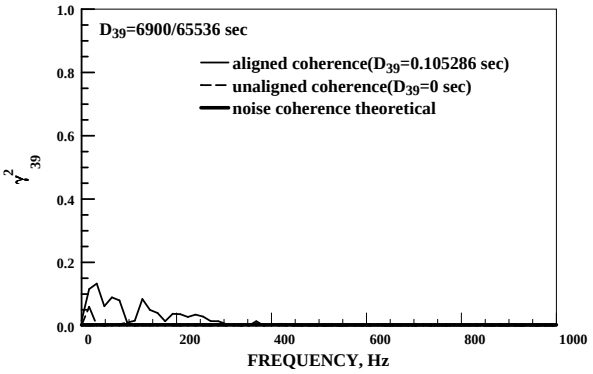

(a) Coherence between microphone at 50^o and combustor pressure sensor, C1P1.

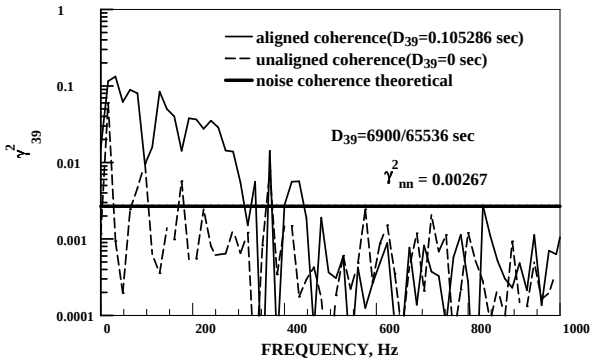

(b) Coherence between microphone at 50^o and combustor pressure sensor, C1P1.

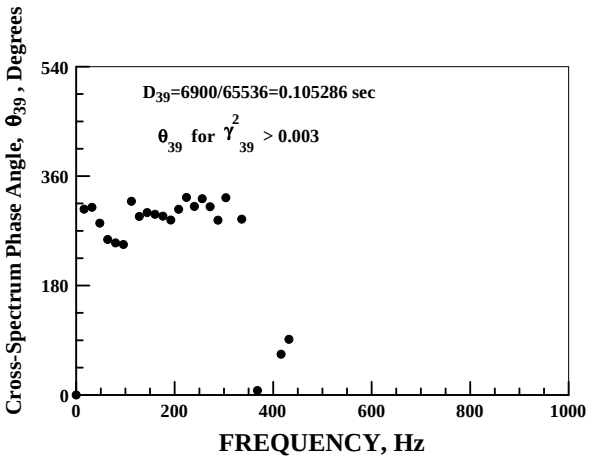

(c) Aligned cross-spectrum phase angle between microphone at 50^o and combustor pressure sensor, C1P1.

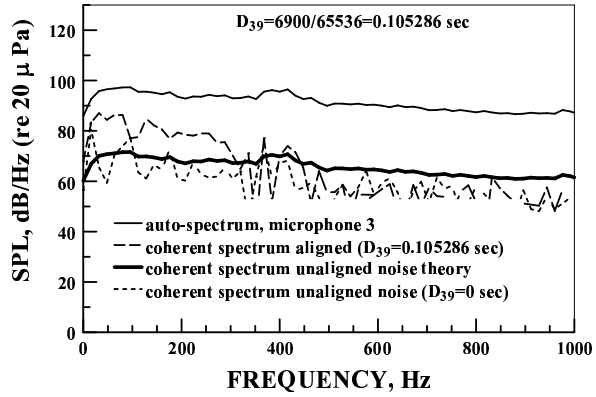

(d) Coherent output power at microphone at 50^o using combustor pressure sensor, C1P1.

Figure 16. TECH977 engine condition power setting of 54 percent microphone at 50^o.

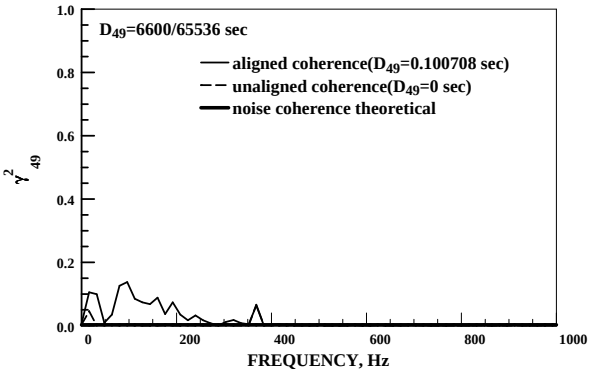

(a) Coherence between microphone at 70^o and combustor pressure sensor, C1P1.

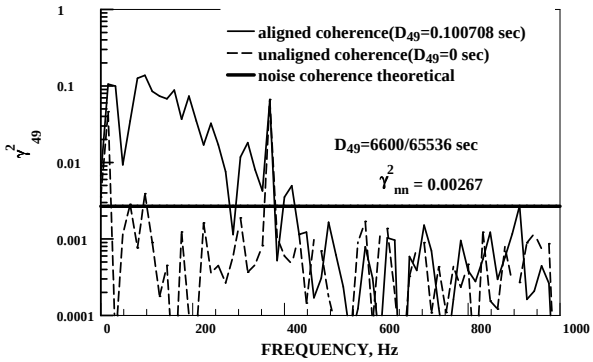

(b) Coherence between microphone at 70^o and combustor pressure sensor, C1P1.

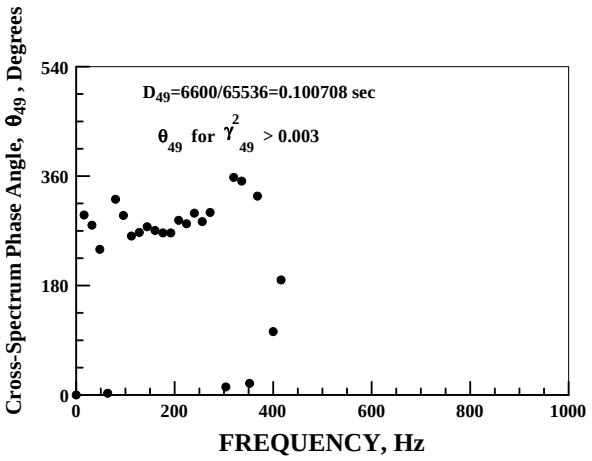

(c) Aligned cross-spectrum phase angle between microphone at 70^o and combustor pressure sensor, C1P1.

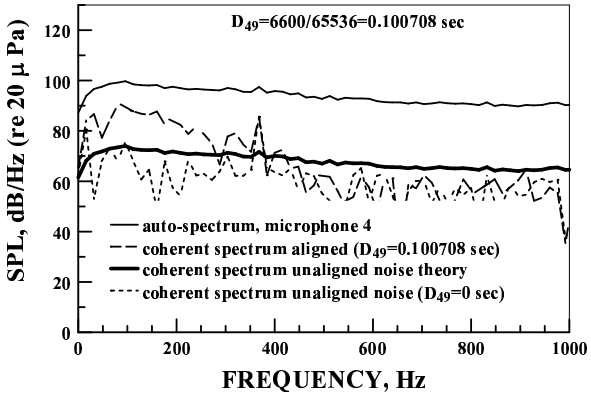

(d) Coherent output power at microphone at 70^o using combustor pressure sensor, C1P1.

Figure 17. TECH977 engine condition power setting of 54 percent microphone at 70^o.

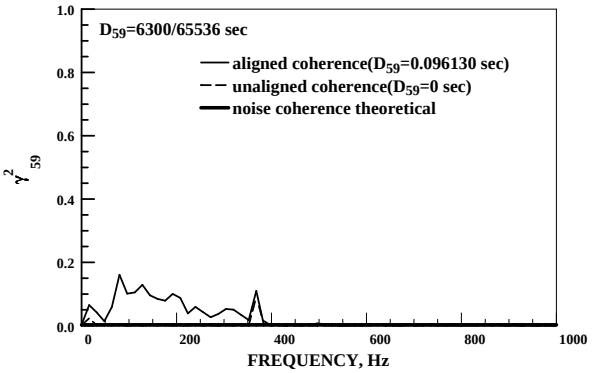

(a) Coherence between microphone at 90^o and combustor pressure sensor, C1P1.

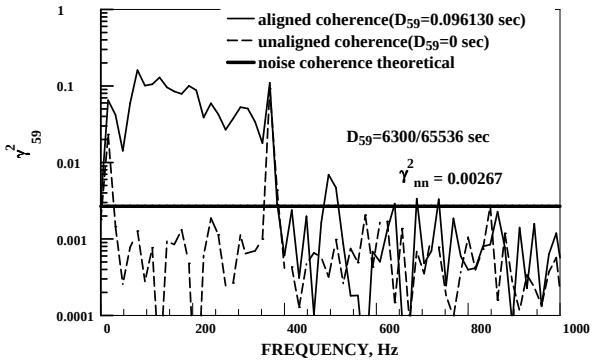

(b) Coherence between microphone at 90^o and combustor pressure sensor, C1P1.

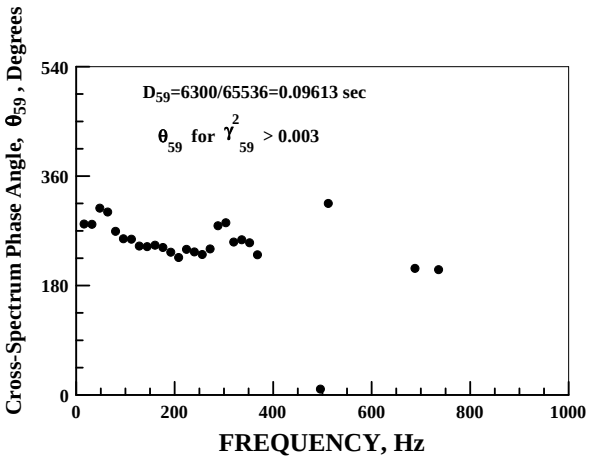

(c) Aligned cross-spectrum phase angle between microphone at 90^o and combustor pressure sensor, C1P1.

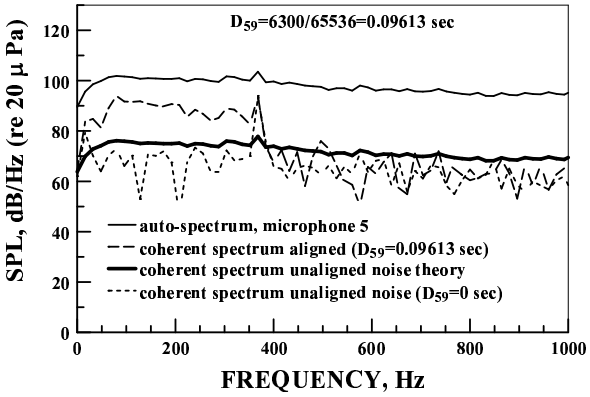

(d) Coherent output power at microphone at 90^o using combustor pressure sensor, C1P1.

Figure 18. TECH977 engine condition power setting of 54 percent microphone at 90^o.

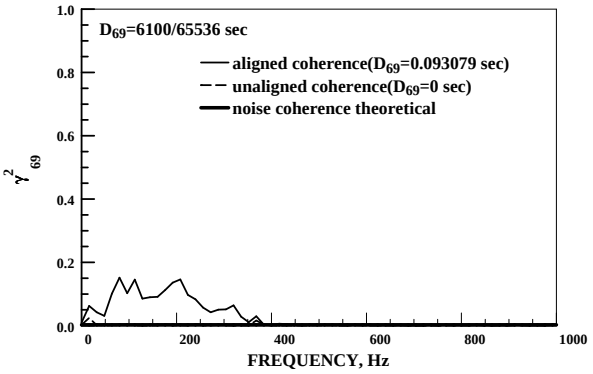

(a) Coherence between microphone at 110^o and combustor pressure sensor, C1P1.

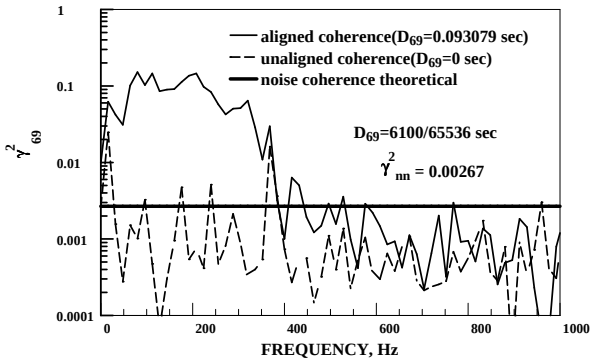

(b) Coherence between microphone at 110^o and combustor pressure sensor, C1P1.

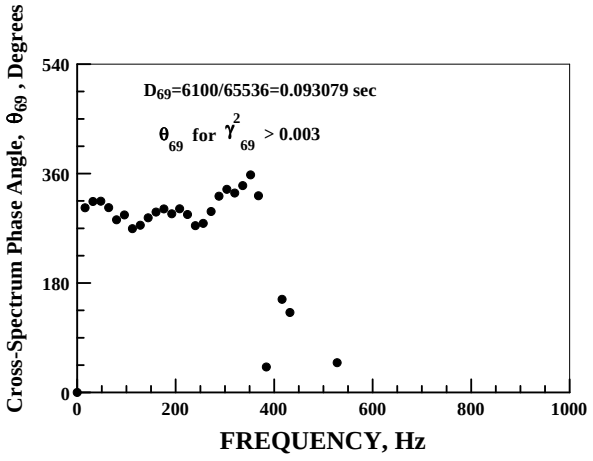

(c) Aligned cross-spectrum phase angle between microphone at 110^o and combustor pressure sensor, C1P1.

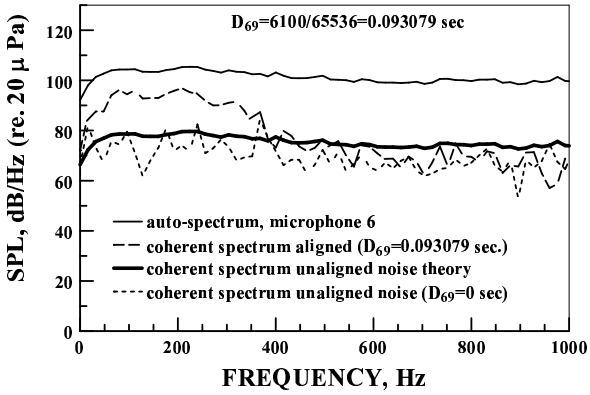

(d) Coherent output power at microphone at 110^o using combustor pressure sensor, C1P1.

Figure 19. TECH977 engine condition power setting of 54 percent microphone at 110^o.

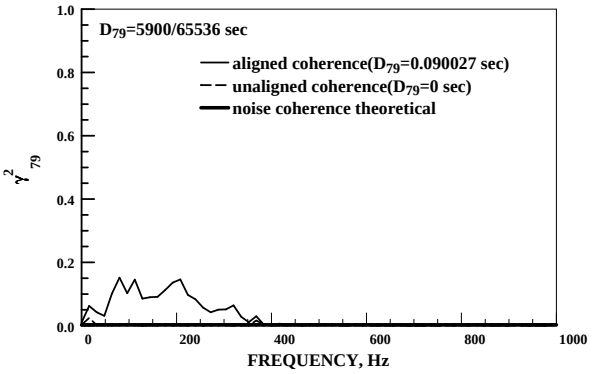

(a) Coherence between microphone at 130^o and combustor pressure sensor, C1P1.

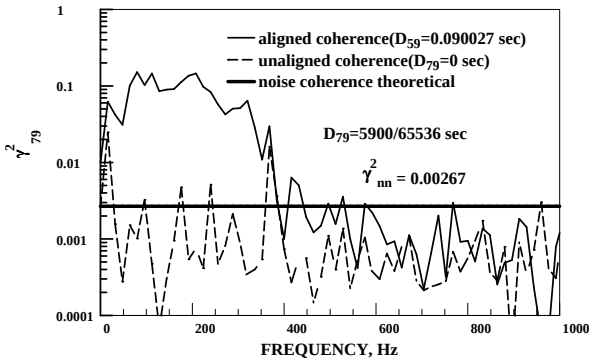

(b) Coherence between microphone at 130^o and combustor pressure sensor, C1P1.

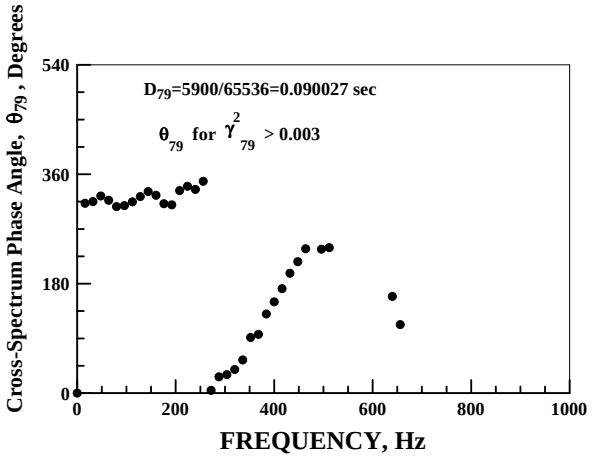

(c) Aligned cross-spectrum phase angle between microphone at 130^o and combustor pressure sensor, C1P1.

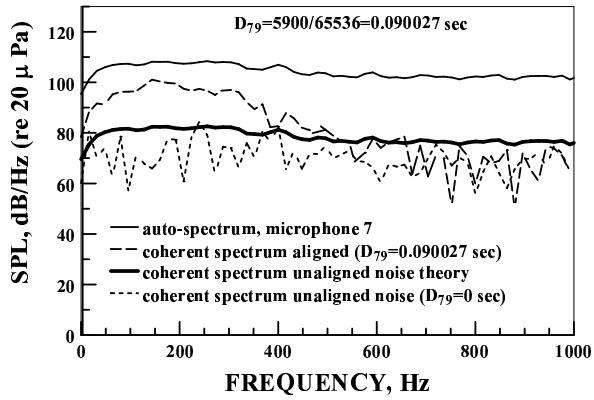

(d) Coherent output power at microphone at 130^o using combustor pressure sensor, C1P1.

Figure 20. TECH977 engine condition power setting of 54 percent microphone at 130^o.

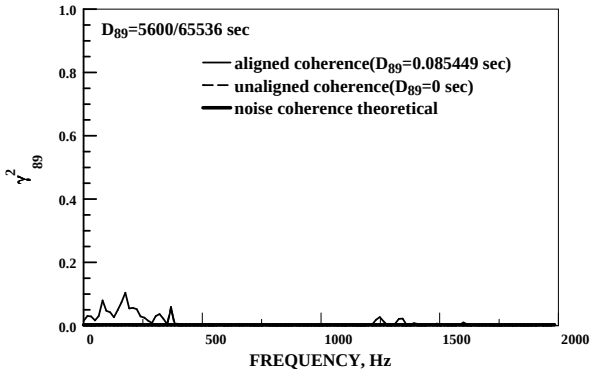

(a) Coherence between microphone at 160^o and combustor pressure sensor, C1P1.

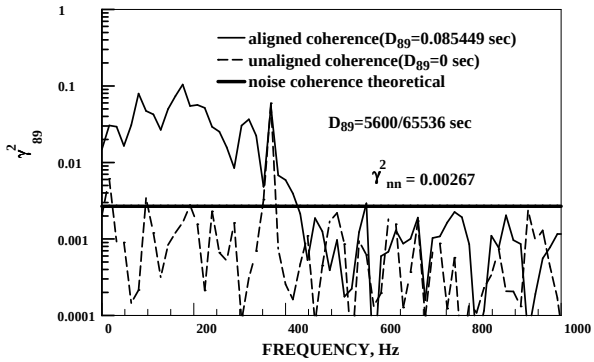

(b) Coherence between microphone at 160^o and combustor pressure sensor, C1P1.

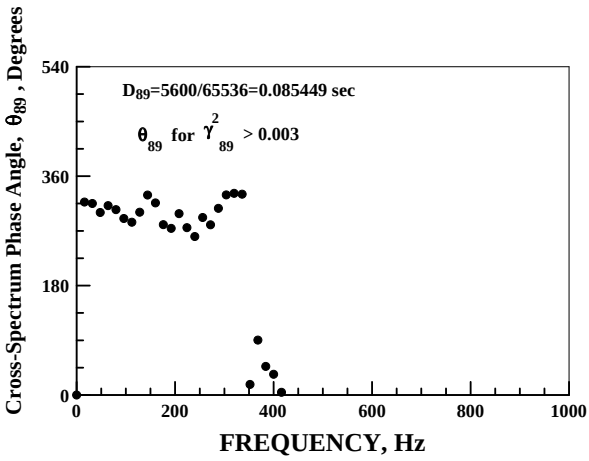

(c) Aligned cross-spectrum phase angle between microphone at 160^o and combustor pressure sensor, C1P1.

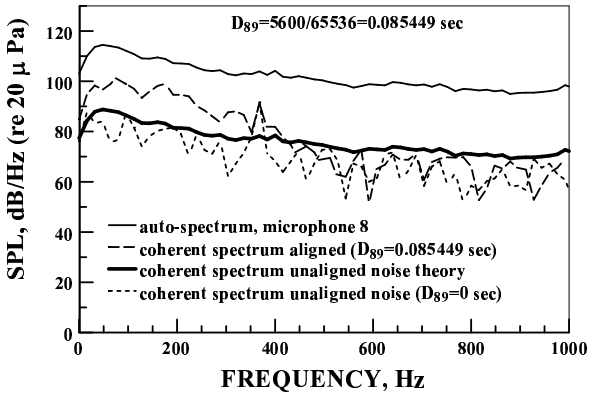

(d) Coherent output power at microphone at 160^o using combustor pressure sensor, C1P1.

Figure 21. TECH977 engine condition power setting of 54 percent microphone at 160^o.

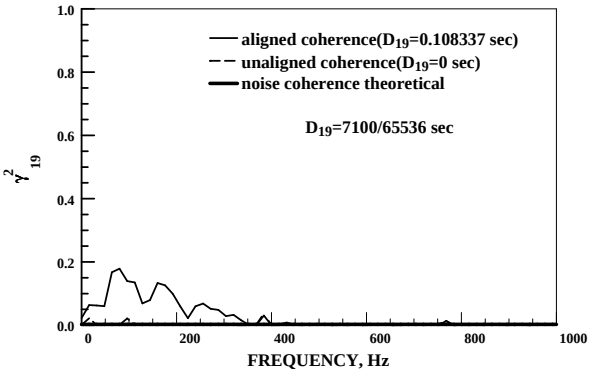

(a) Coherence between microphone at 10^o and C1P1 combustor pressure sensor.

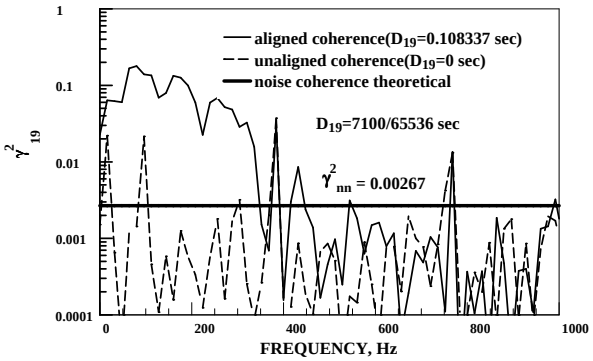

(b) Coherence between microphone at 10^o and C1P1 combustor pressure sensor.

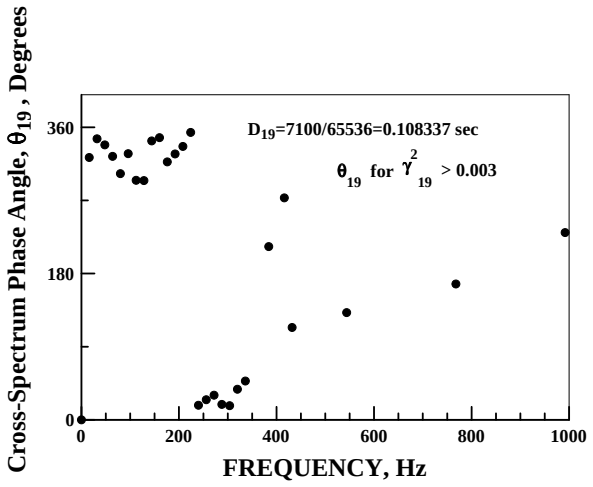

(c) Aligned cross-spectrum phase angle between microphone at 10^o and C1P1 combustor pressure sensor.

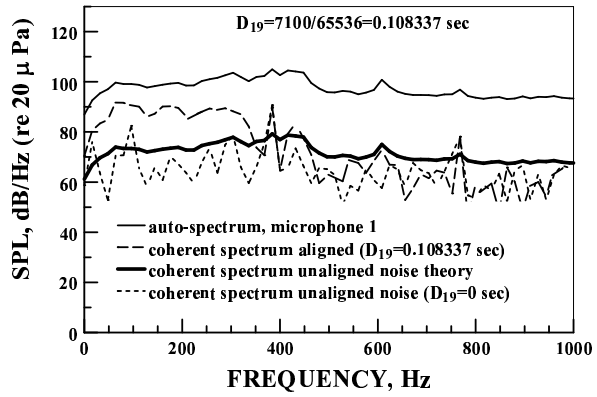

(d) Coherent output power at microphone at 10^o using C1P1 combustor pressure sensor.

Figure 22. TECH977 engine condition power setting of 60 percent microphone at 10^o.

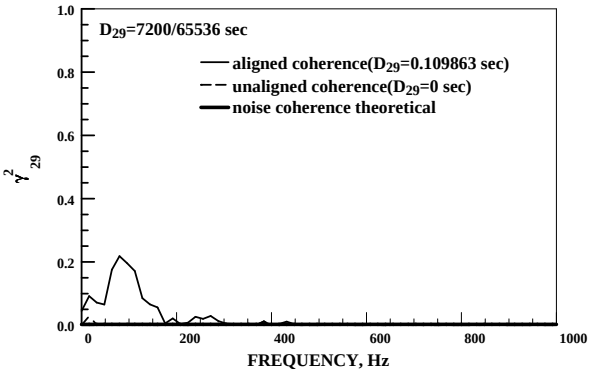

(a) Coherence between microphone at 30^o and C1P1 combustor pressure sensor.

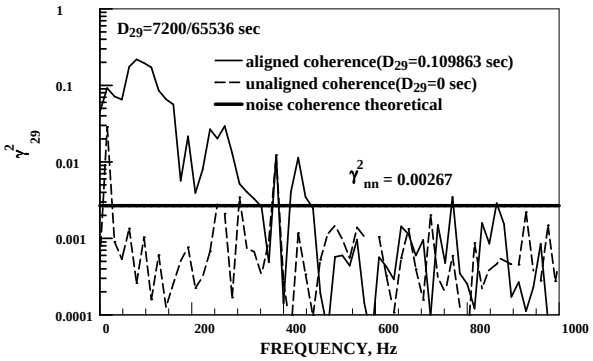

(b) Coherence between microphone at 30^o and C1P1 combustor pressure sensor.

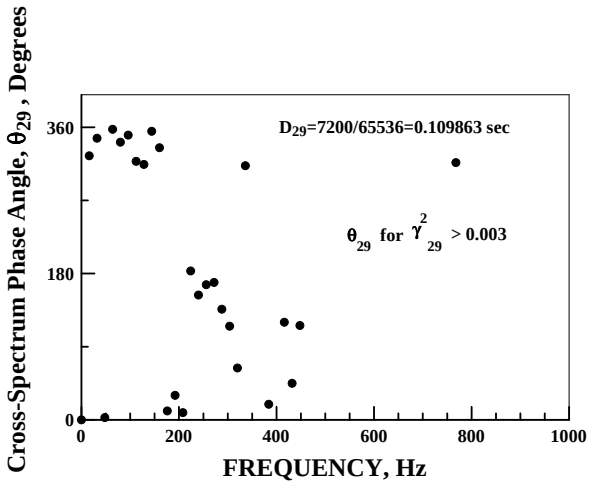

(c) Aligned cross-spectrum phase angle between microphone at 30^o and C1P1 combustor pressure sensor.

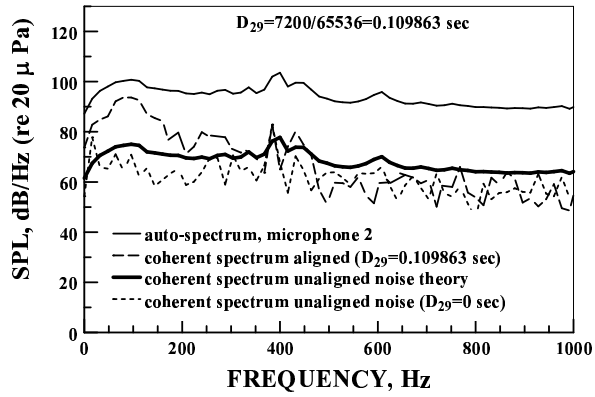

(d) Coherent output power at microphone at 30^o using C1P1 combustor pressure sensor.

Figure 23. TECH977 engine condition power setting of 60 percent microphone at 30^o.

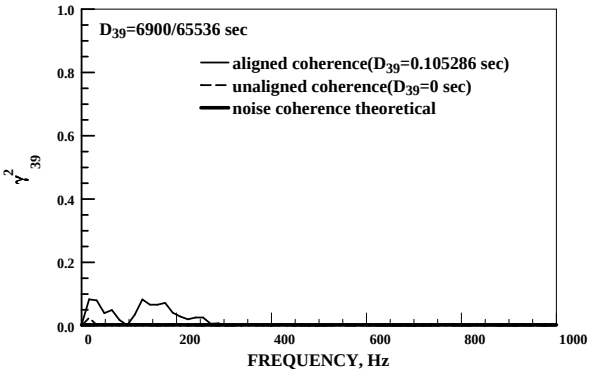

(a) Coherence between microphone at 50^o and C1P1 combustor pressure sensor.

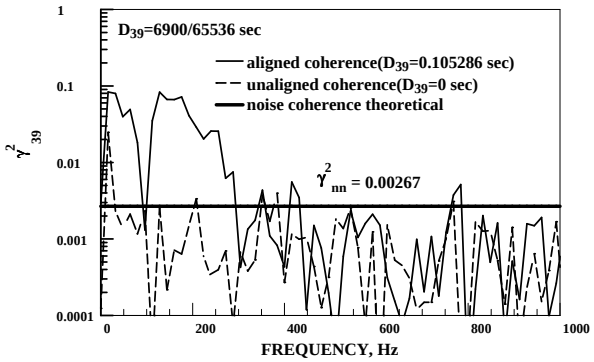

(b) Coherence between microphone at 50^o and C1P1 combustor pressure sensor.

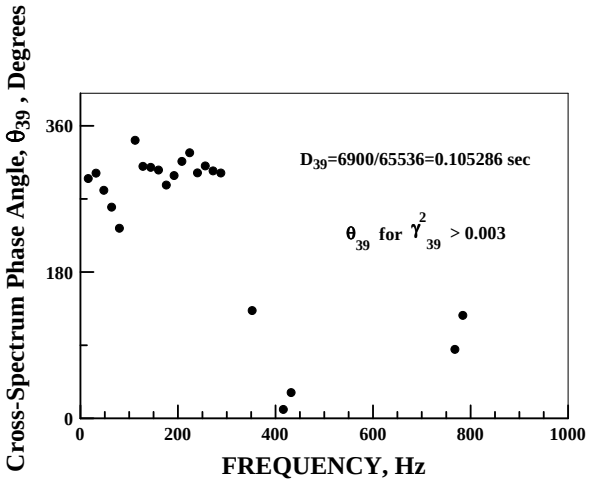

(c) Aligned cross-spectrum phase angle between microphone at 50^o and C1P1 combustor pressure sensor.

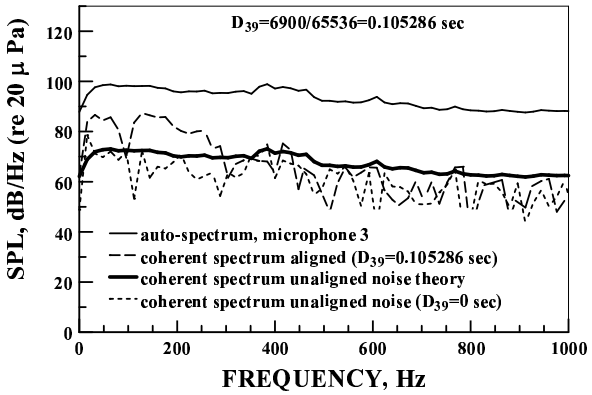

(d) Coherent output power at microphone at 50^o using C1P1 combustor pressure sensor.

Figure 24. TECH977 engine condition power setting of 60 percent microphone at 50^o.

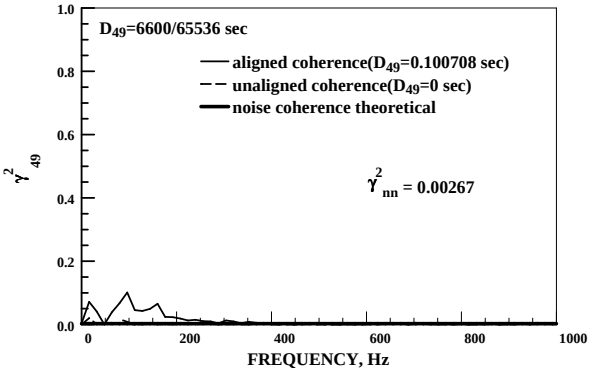

(a) Coherence between microphone at 70^o and C1P1 combustor pressure sensor.

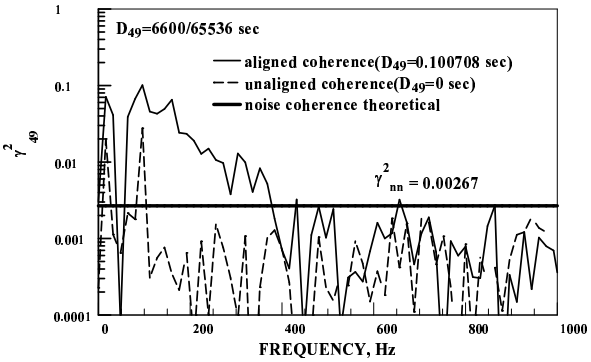

(b) Coherence between microphone at 70^o and C1P1 combustor pressure sensor.

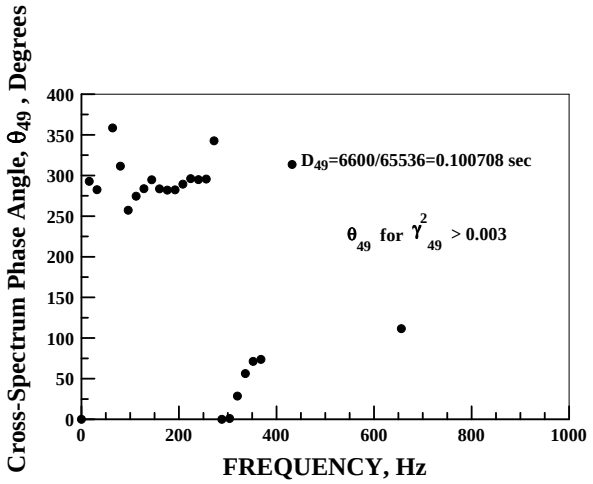

(c) Aligned cross-spectrum phase angle between microphone at 70^o and C1P1 combustor pressure sensor.

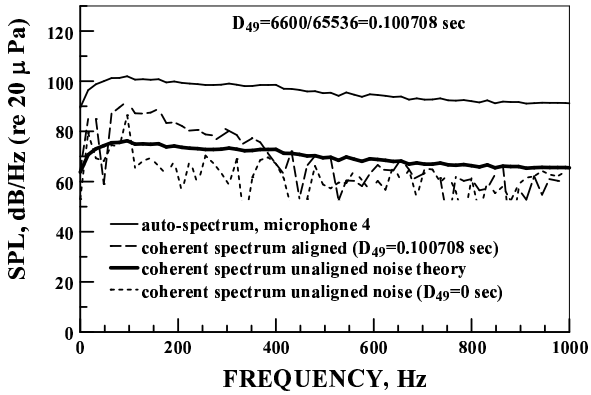

(d) Coherent output power at microphone at 70^o using C1P1 combustor pressure sensor.

Figure 25. TECH977 engine condition power setting of 60 percent microphone at 70^o.

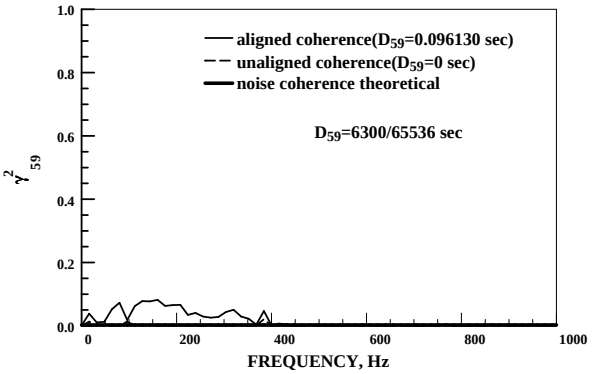

(a) Coherence between microphone at 90^o and C1P1 combustor pressure sensor.

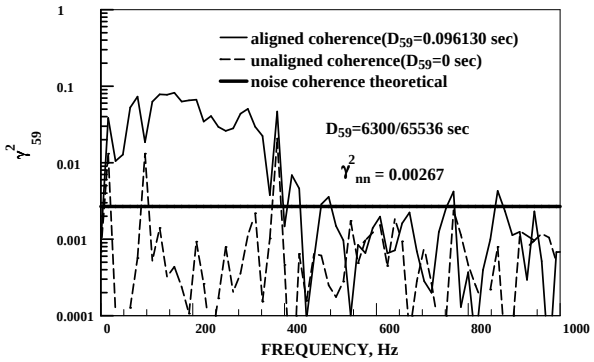

(b) Coherence between microphone at 90^o and C1P1 combustor pressure sensor.

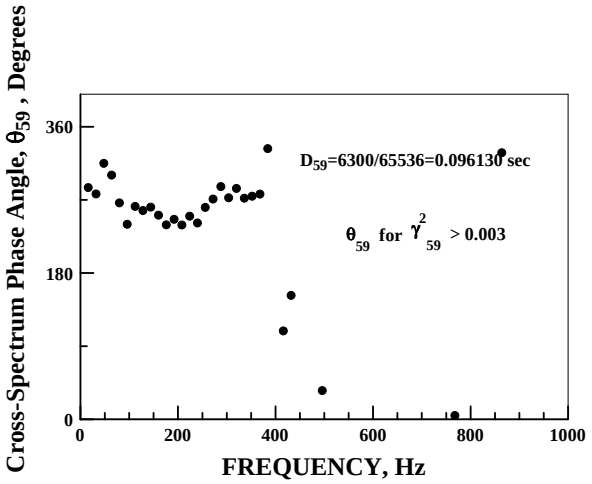

(c) Aligned cross-spectrum phase angle between microphone at 90^o and C1P1 combustor pressure sensor.

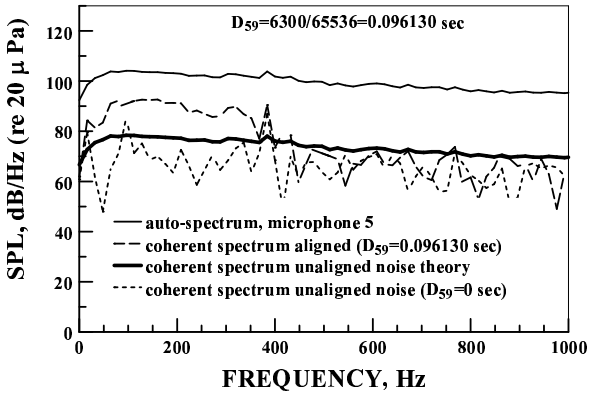

(d) Coherent output power at microphone at 90^o using C1P1 combustor pressure sensor.

Figure 26. TECH977 engine condition power setting of 60 percent microphone at 90^o.

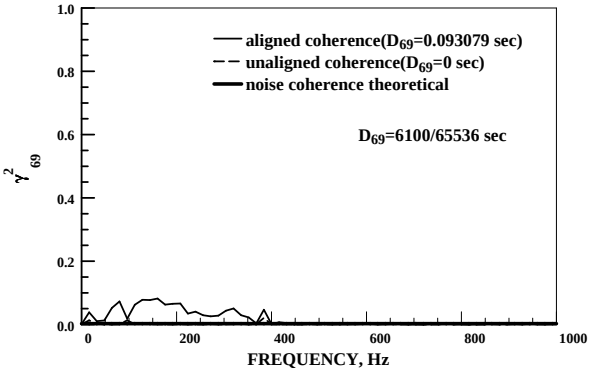

(a) Coherence between microphone at 110^o and C1P1 combustor pressure sensor.

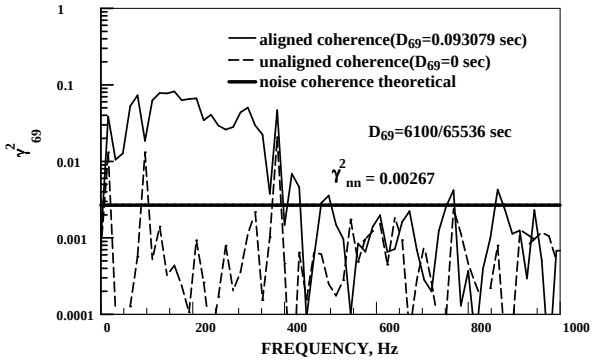

(b) Coherence between microphone at 110^o and C1P1 combustor pressure sensor.

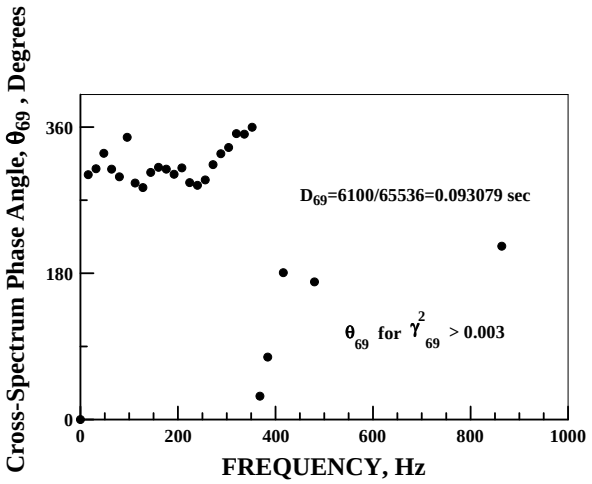

(c) Aligned cross-spectrum phase angle between microphone at 110^o and C1P1 combustor pressure sensor.

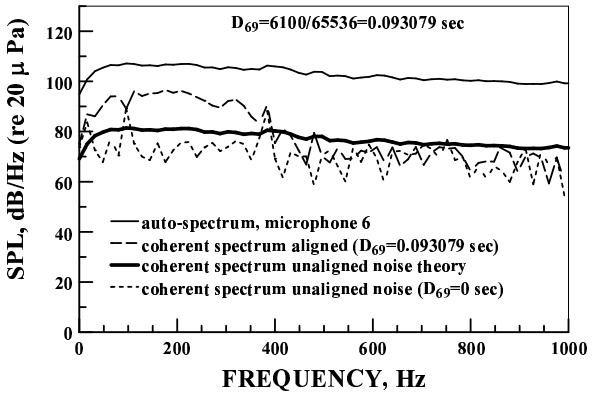

(d) Coherent output power at microphone at 110^o using C1P1 combustor pressure sensor.

Figure 27. TECH977 engine condition power setting of 60 percent microphone at 110^o.

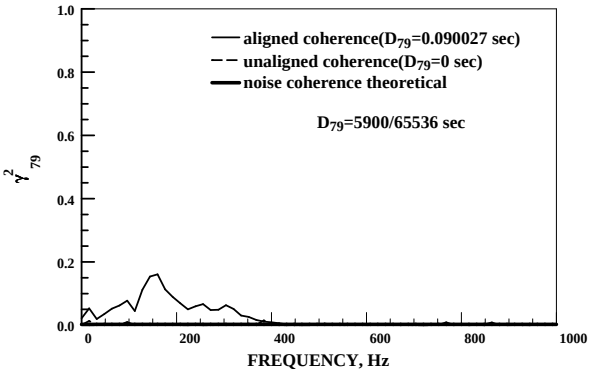

(a) Coherence between microphone at 130^o and C1P1 combustor pressure sensor.

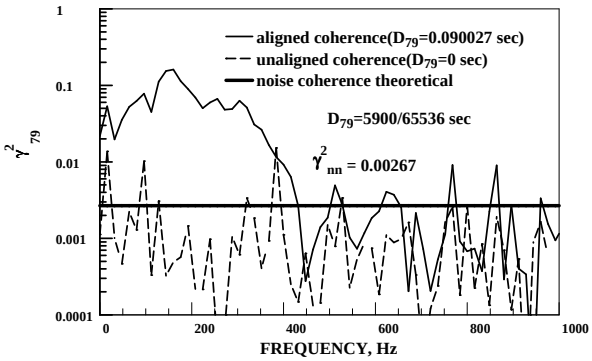

(b) Coherence between microphone at 130^o and C1P1 combustor pressure sensor.

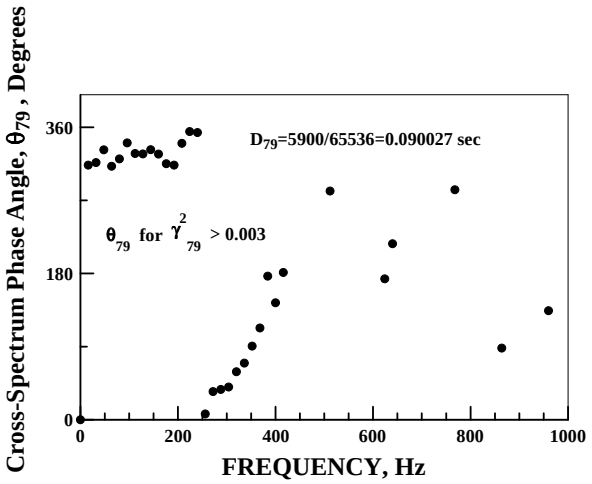

(c) Aligned cross-spectrum phase angle between microphone at 130^o and C1P1 combustor pressure sensor.

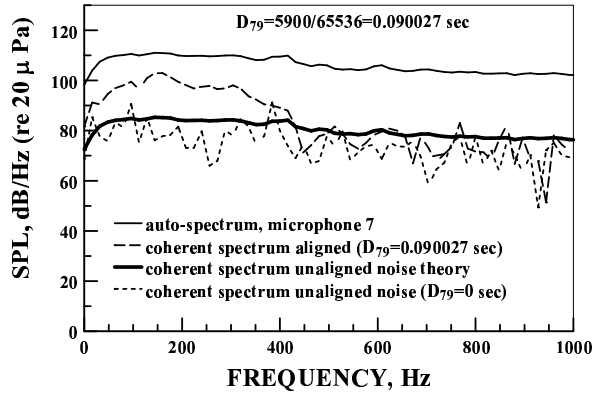

(d) Coherent output power at microphone at 130^o using C1P1 combustor pressure sensor.

Figure 28. TECH977 engine condition power setting of 60 percent microphone at 130^o.

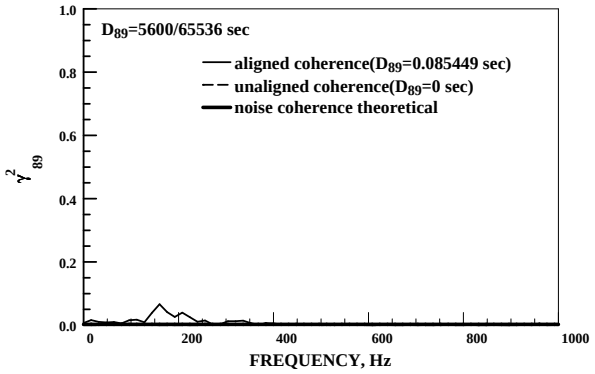

(a) Coherence between microphone at 160^o and C1P1 combustor pressure sensor.

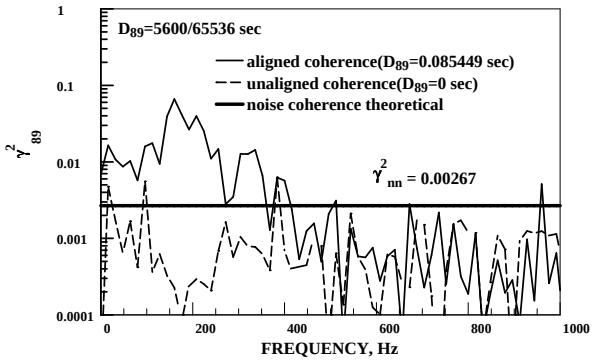

(b) Coherence between microphone at 160^o and C1P1 combustor pressure sensor.

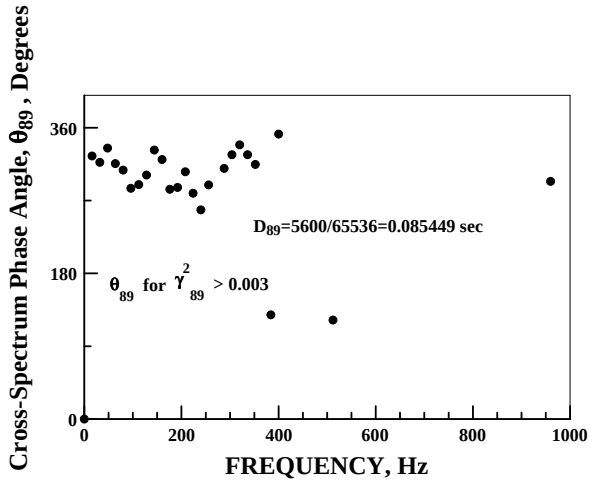

(c) Aligned cross-spectrum phase angle between microphone at 160^o and C1P1 combustor pressure sensor.

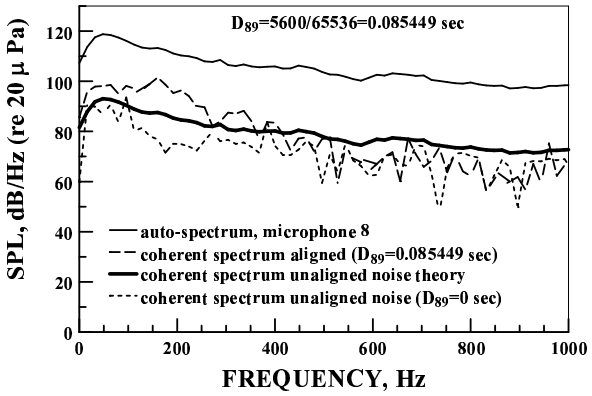

(d) Coherent output power at microphone at 160^o using C1P1 combustor pressure sensor.

Figure 29. TECH977 engine condition power setting of 60 percent microphone at 160^o.

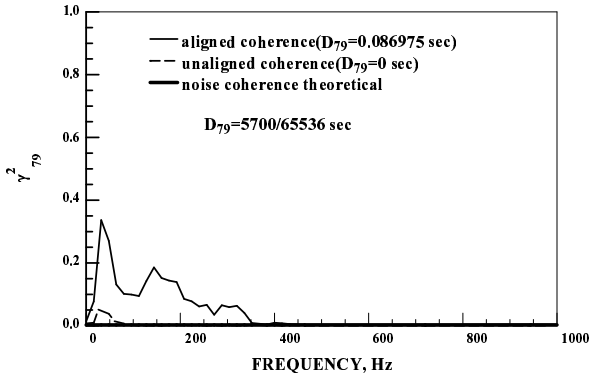

(a) Coherence between microphone at 130^o and C1P1 combustor pressure sensor.

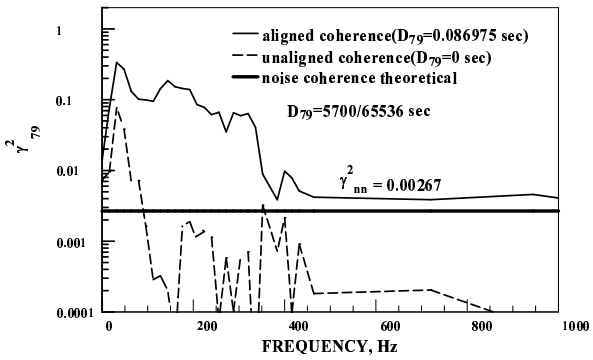

(b) Coherence between microphone at 130^o and C1P1 combustor pressure sensor.

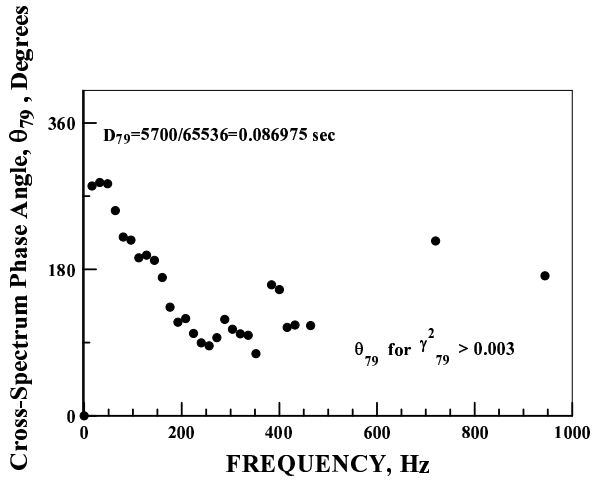

(c) Aligned cross-spectrum phase angle between microphone at 130^o and C1P1 combustor pressure sensor.

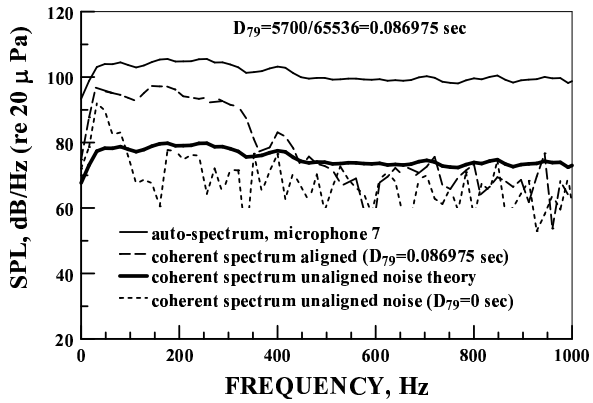

(d) Coherent output power at microphone at 130^o using C1P1 combustor pressure sensor.

Figure 30. $D_T = 5700/65536 = .086975$ **TECH977 engine condition power setting of 48 percent microphone at** 130^o**.**

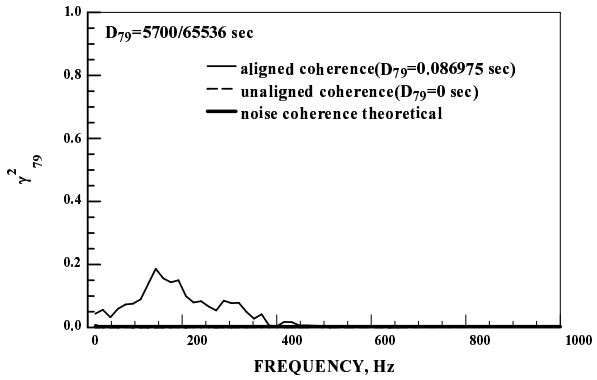

(a) Coherence between microphone at 130^o and combustor pressure sensor, C1P1.

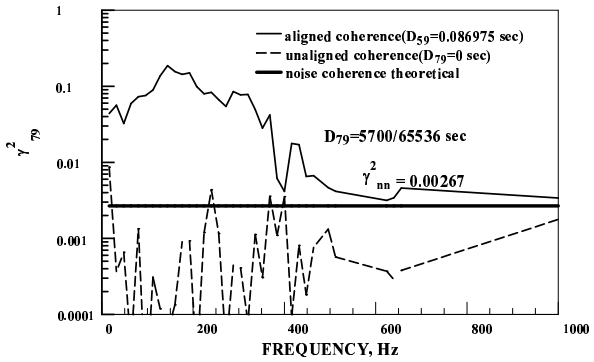

(b) Coherence between microphone at 130^o and combustor pressure sensor, C1P1.

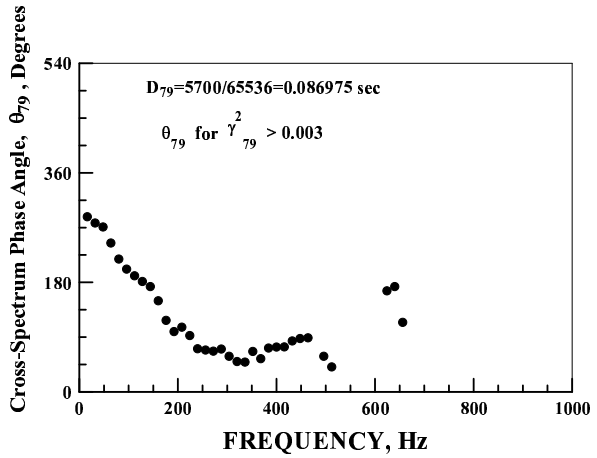

(c) Aligned cross-spectrum phase angle between microphone at 130^o and combustor pressure sensor, C1P1.

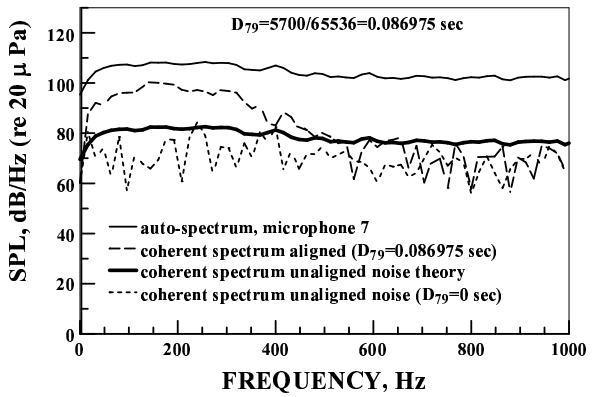

(d) Coherent output power at microphone at 130^o using combustor pressure sensor, C1P1.

Figure 31. $D_T = 5700/65536 = .086975$ **TECH977 engine condition power setting of 54 percent microphone at** 130^o**.**

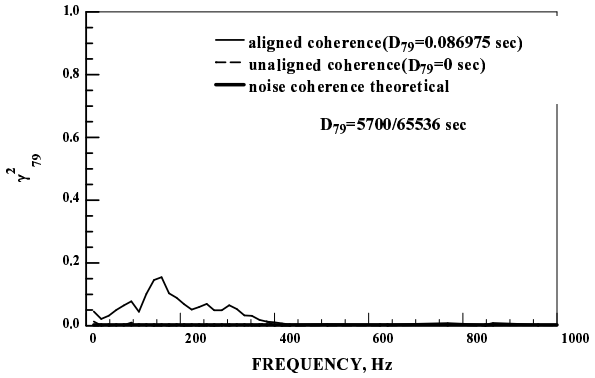

(a) Coherence between microphone at 130^o and C1P1 combustor pressure sensor.

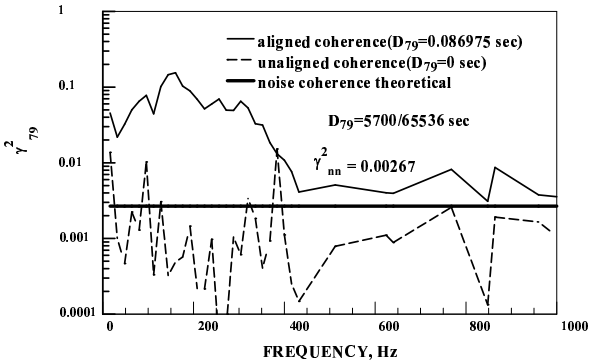

(b) Coherence between microphone at 130^o and C1P1 combustor pressure sensor.

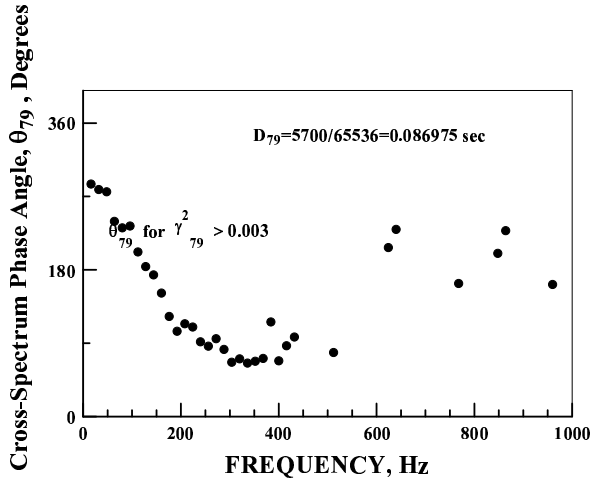

(c) Aligned cross-spectrum phase angle between microphone at 130^o and C1P1 combustor pressure sensor.

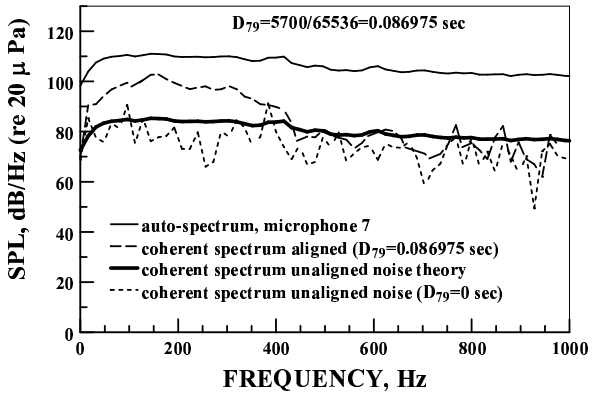

(d) Coherent output power at microphone at 130^o using C1P1 combustor pressure sensor.

Figure 32. $D_T = 5700/65536 = .086975$ **TECH977 engine condition power setting of 60 percent microphone at** 130^o**.**

REPORT DOCUMENTATION PAGE		Form Approved OMB No. 0704-0188

1. REPORT DATE *(DD-MM-YYYY)*	2. REPORT TYPE	3. DATES COVERED *(From - To)*
01-05-2008	Technical Memorandum	

4. TITLE AND SUBTITLE
Spectral Separation of the Turbofan Engine Coherent Combustion Noise Component

5a. CONTRACT NUMBER

5b. GRANT NUMBER

5c. PROGRAM ELEMENT NUMBER

6. AUTHOR(S)
Miles, Jeffrey, Hilton

5d. PROJECT NUMBER

5e. TASK NUMBER

5f. WORK UNIT NUMBER
WBS 561581.02.08.03.18.03

7. PERFORMING ORGANIZATION NAME(S) AND ADDRESS(ES)
National Aeronautics and Space Administration
John H. Glenn Research Center at Lewis Field
Cleveland, Ohio 44135-3191

8. PERFORMING ORGANIZATION REPORT NUMBER
E-16398

9. SPONSORING/MONITORING AGENCY NAME(S) AND ADDRESS(ES)
National Aeronautics and Space Administration
Washington, DC 20546-0001

10. SPONSORING/MONITORS ACRONYM(S)
NASA

11. SPONSORING/MONITORING REPORT NUMBER
NASA/TM-2008-215157; AIAA-2008-50

12. DISTRIBUTION/AVAILABILITY STATEMENT
Unclassified-Unlimited
Subject Category: 71
Available electronically at http://gltrs.grc.nasa.gov
This publication is available from the NASA Center for AeroSpace Information, 301-621-0390

13. SUPPLEMENTARY NOTES

14. ABSTRACT
The core noise components of a dual spool turbofan engine (Honeywell TECH977) were separated by the use of a coherence function. A source location technique based on adjusting the time delay between the combustor pressure sensor signal and the far-field microphone signal to maximize the coherence and remove as much variation of the phase angle with frequency as possible was used. While adjusting the time delay to maximize the coherence and minimize the cross spectrum phase angle variation with frequency, the discovery was made that for the 130° microphone a 90.027 ms time shift worked best for the frequency band from 0 to 200 Hz while a 86.975 ms time shift worked best for the frequency band from 200 to 400 Hz. Since the 0 to 200 Hz band signal took more time to travel the same distance, it is slower than the 200 to 400 Hz band signal. This suggests the 0 to 200 Hz coherent cross spectral density band is partly due to indirect combustion noise attributed to hot spots interacting with the turbine. The signal in the 200 to 400 Hz frequency band is attributed mostly to direct combustion noise.

15. SUBJECT TERMS
Jet aircraft noise; Acoustic measurement; Combustion noise; Signal detection; Signal analysis core

16. SECURITY CLASSIFICATION OF:			17. LIMITATION OF ABSTRACT	18. NUMBER OF PAGES	19a. NAME OF RESPONSIBLE PERSON
a. REPORT	b. ABSTRACT	c. THIS PAGE			STI Help Desk (email:help@sti.nasa.gov)
U	U	U	UU	53	19b. TELEPHONE NUMBER *(include area code)* 301-621-0390